Microscopic description of the ^{2}H(α, γ)^{6}Li radiative capture reaction

Alexander S. Solovyev [*]
Dukhov Automatics Research Institute (VNIIA), 22 Sushchevskaya street, Moscow 127055, Russia

The ^{2}H(α, γ)^{6}Li radiative capture responsible for the ^{6}Li production during the big-bang nucleosynthesis is comprehensively studied within a microscopic approach. The approach implements microscopically clustering aspects of nuclear structure and dynamics in an oscillator-basis representation. The total astrophysical S factor of the reaction is calculated. All allowed partial electric quadrupole and magnetic dipole transitions between the ^{4}He $+ ^2$H continuum and the ^{6}Li ground state are considered in the standard long-wavelength limit. Isospin-forbidden electric dipole transitions are taken into account in two ways. The first method is based on the expression for the electric dipole operator at the leading order of the long-wavelength approximation with the usage of the exact-mass prescription. In the second method, this operator is written at the first order beyond the leading-order approximation. Contributions of the transitions are compared to each other. The ^{4}He $+ ^2$H nuclear phase shifts for the initial channels of the considered reaction are computed. Important properties of the ^{6}Li nucleus, such as the breakup threshold, the asymptotic normalization constants, and the electric quadrupole moment are also described. Deformation effects and their manifestations in ^{6}Li are discussed. The obtained results are shown to be in good agreement with a large set of experimental data.

I. INTRODUCTION

Nuclear reactions responsible for production and destruction of lithium isotopes are of great interest for astrophysical applications because their cross sections (astrophysical S factors) serve as input. At the present time, there is, in particular, the so-called "lithium depletion" problem in nuclear astrophysics. This problem is related to the abundance of the lithium isotopes in the Universe and includes two puzzles. The reason for the first lithium puzzle is a discrepancy between predictions of the big-bang nucleosynthesis model and astronomical observations in metal-poor halo stars for the primordial ^{7}Li/H ratio. The model predictions $(5.24^{+0.71}_{-0.67}) \times 10^{-10}$ [1], $(4.56-5.34) \times 10^{-10}$ [2], $(5.61 \pm 0.26) \times 10^{-10}$ [3,4], 4.648×10^{-10} [5], and $(4.68 \pm 0.67) \times 10^{-10}$ [5] are about three to four times larger than values of $(1.23^{+0.68}_{-0.32}) \times 10^{-10}$ [6] and $1.58^{+0.35}_{-0.28}) \times 10^{-10}$ [7] from analyses of the observational data. The second lithium puzzle is caused by a disagreement between estimations for the primordial abundance ratio of the lithium isotopes (^{6}Li/^{7}Li) obtained from the big-bang nucleosynthesis model ($\sim 10^{-5}$) [2,5,8] and from an analysis of astrophysical data on the lithium abundance in metal-poor halo stars ($\sim 5 \times 10^{-2}$) [9]. The discrepancy is about three orders of magnitude. Nevertheless, it should be noted that findings of works [10–12] demonstrate that the second lithium puzzle could be weakened.

The ^{3}H(α, γ)^{7}Li and ^{3}He(α, γ)^{7}Be radiative captures are assumed to be the key reactions for a calculation of the ^{7}Li primordial abundance. A recent theoretical study of these reactions was comprehensively performed within microscopic approaches in works [13,14] where references to a large number of previous experimental and theoretical investigations can be found. The corresponding review and discussions are also given in Refs. [13,14].

In turn, the ^{2}H(α, γ)^{6}Li radiative capture at energies from 50 keV up to 400 keV is responsible for the big-bang nucleosynthesis of the ^{6}Li nuclei. Experimental studies of this reaction at the astrophysically relevant energies are very difficult because of the Coulomb barrier, which exponentially decreases the reaction cross section. In works [15–22], data on the ^{2}H(α, γ)^{6}Li reaction are deduced from experimental measurements. These experiments cover a wide energy range. However, the data have some scatter and large uncertainties at the astrophysical energies. That is why extrapolations based on theoretical calculations are required.

The ^{2}H(α, γ)^{6}Li theoretical studies are also very challenging. As it is well known, electric dipole (E1) and magnetic dipole (M1) transitions for radiative capture reactions between so-called self-conjugate nuclei, for which the number of neutrons coincides with the number of protons, are strongly suppressed due to an isospin selection rule (the isotopic suppression). At the leading order of the long-wavelength limit, which is a good approximation for a radiative-capture description at astrophysical energies, E1 transitions between zero-isospin states for self-conjugate nuclei and systems composed of them are isospin forbidden. Electric quadrupole (E2) transitions dominate in this case. However, there are various E1 corrections that should be taken into account because they may become important in some cases. An analysis of these corrections is a difficult task, especially from the microscopic viewpoint.

[*]alexander.solovyev@mail.ru

In Refs. [15,17], calculations of the ^{2}H$(\alpha, \gamma)^6$Li total cross section were performed in a direct capture model (DCM). A three-body approach and a potential cluster model (PCM) were respectively applied in Refs. [19,20]. The cross section of the ^{2}H$(\alpha, \gamma)^6$Li reaction caused by the E2 transitions only was calculated using the PCM in Ref. [23], the PCM combined with the resonating group model (RGM) in Ref. [24], and the DCM in Refs. [25,26]. In Ref. [27], the relative intensity of the E1 versus E2 radiation in the ^{2}H$(\alpha, \gamma)^6$Li reaction was estimated using simple versions of cluster and shell models for the ^{6}Li nucleus and perturbation theory for a description of the Coulomb polarizability of the deuteron. The obtained corrections to the E1 radiation were appeared to be small enough but not negligible ones. Various E1 corrections were also considered in work [28] within the PCM. It was shown that the so-called prescription of exact masses (PEM) led to the E1 transitions of the same order as the E2 ones for the ^{2}H$(\alpha, \gamma)^6$Li reaction at very low energies. The former ones even turned out larger in magnitude than the latter ones with the energy decrease. In other studies, the PEM was employed to take into account the forbidden E1 transitions for the considered reaction in the multichannel RGM [29], in the framework of a multicluster dynamic model with Pauli projection [30], and within the two-body PCM based on a concept of the asymptotic normalization coefficient (ANC) [31–34]. A microscopic three-cluster generator coordinate method was used in Ref. [35] to analyze the E2 contribution to the ^{2}H$(\alpha, \gamma)^6$Li total astrophysical S factor with different conditions of the calculations. In Refs. [36,37], the total astrophysical S factor was computed using a hybrid approach where the ^{6}Li bound state wave function was generated by the variational Monte Carlo (VMC) method from realistic potentials. The same potentials were used for the initial scattering state to generate the ground-state VMC solution for the α particle and to solve almost exactly a two-nucleon Schrödinger equation for the deuteron, whereas the α-d relative motion wave function followed from a Schrödinger equation with a phenomenological two-body potential. In fact, an *ab initio* description of the final state was combined with a phenomenological two-body description of the initial states. It was shown that the main contribution to the total E1 capture was caused by the relativistic center-of-energy correction, which was interpreted in the work [36] as an analog of the PEM. In Refs. [38–43], calculations for the ^{2}H$(\alpha, \gamma)^6$Li total astrophysical S factor were performed in the framework of various two-body PCM, using the PEM for the E1 transitions. Finally, the considered reaction was studied in a three-body cluster model in Refs. [44–47]. Only in the frame of the PEM, the total astrophysical S-factor data were reproduced in Ref. [44]. Meanwhile, it was suggested in Refs. [45–47] that the forbidden E1 transitions were mainly caused by the presence of isotriplet component admixtures in the wave functions. Moreover, some criticism of the PEM was undertaken in Ref. [46].

Thus, there are only a few microscopic studies devoted to ^{2}H$(\alpha, \gamma)^6$Li. Those studies were performed a long time ago and not devoid of certain drawbacks. In order to broaden the knowledge and to find reliable answers to open questions,

new microscopic investigations of this reaction are obviously worthwhile.

It should be noted that the description of nuclear spectroscopy and properties of ^{6}Li and the d-α elastic scattering also attracts attention of researchers, despite a long story of the investigations. Nowadays, there are various approaches to this problem. In recent works, both advanced *ab initio* methods and simple two-body models have been developing. The *ab initio* no-core shell model (NCSM) combined with the RGM (NCSM/RGM) [48] and the NCSM with continuum [49] were applied to describe the ^{6}Li states and the d-α scattering. In Ref. [50], the *ab initio* no-core full configuration approach was implemented to solve for ^{6}Li properties. A feed-forward artificial neural network method was proposed in Ref. [51] as an extrapolation tool to obtain the ground-state energy and the ground-state point-proton root-mean-square (rms) radius along with their extrapolation uncertainties based upon NCSM results in readily solved basis spaces and was applied to ^{6}Li. In Ref. [52], the ^{6}Li nucleus and the d-α scattering were considered by an effective two-body clusterization method based on Sturmian expansion solutions of the Lippmann-Schwinger equations. A method of analytical continuation of elastic scattering data at positive energies to the negative-energy region to obtain information about the features of bound states was discussed and applied to extract some ^{6}Li bound-state properties in works [53–56]. In Ref. [57], an exactly solvable simple potential model with a δ-shell potential was used to revisit bound states, resonances, and elastic scattering in light-ion systems, including $\alpha + d$. It is clear from what has been said above that not only the ^{2}H$(\alpha, \gamma)^6$Li reaction, but also its initial and final channels are individually of interest for many modern studies.

The aim of the present paper is to study thoroughly the ^{2}H$(\alpha, \gamma)^6$Li radiative capture reaction from the microscopic viewpoint. The developed approach is based on a microscopic implementation of clustering aspects of nuclear structure and dynamics with the use of oscillator-basis expansions for the relative motion wave functions of the clusters and a realistic effective nuclear potential for the nucleon-nucleon (NN) interaction. The energy dependence of the total astrophysical S factor is calculated. The contributions of all possible E1, E2, and M1 captures are taken into account. The ^{2}H$(\alpha, \alpha)^2$H elastic scattering and the ^{6}Li properties are also considered. In fact, a unified microscopic description of nuclear structure and dynamics of the six-nucleon ^{4}He $+$ ^{2}H system is performed. The discrete spectrum and the continuum of this system, including the electromagnetic transitions between them, are treated in a consistent way within the implemented approach.

It should be emphasized that approaches based on oscillator-basis expansions are effective tools in modern nuclear physics for solving many important problems of nuclear theory. In particular, it is clearly seen from works [13,14,58–69] where various aspects of oscillator-basis calculations are considered.

II. FORMALISM OF THE APPROACH

Cluster concept of nuclear structure and dynamics is known to be a superb physical assumption for a variety of light

nuclei. Clustering in light nuclei is confirmed by many experimental facts and theoretical estimations (for example, see a recent review [70] and references cited therein). According to the nuclear cluster model, nucleons in nuclei spend a significant fraction of their time in various substructures called nuclear clusters. The total wave function of an A-nucleon system studied in a microscopic two-cluster model should be written in the form of a fully antisymmetrized product of the translationally invariant intrinsic wave functions $\phi^{(1)}$ and $\phi^{(2)}$ of the clusters and the wave function $f(\mathbf{q})$ of their relative motion,

$$\Psi = \mathcal{A}\{\phi^{(1)}\phi^{(2)}f(\mathbf{q})\}, \tag{1}$$

where $\mathcal{A}$ is the antisymmetrization operator, and $\mathbf{q}$ is the relative vector. If the intrinsic cluster wave functions are supposed to be fixed, the problem is reduced to finding the relative motion wave function $f(\mathbf{q})$.

In order to reformulate the problem, one can make use of an expansion in series,

$$f(\mathbf{q}) = \sum_{\nu l m} C_{\nu l m} f_{\nu l m}(\mathbf{q}), \tag{2}$$

of the oscillator functions,

$$f_{\nu l m}(\mathbf{q}) = N_{\nu l}\,\bar{q}^l L_{(\nu-l)/2}^{(l+1/2)}(\bar{q}^2)\,\exp\left(-\bar{q}^2/2\right)Y_{lm}(\mathbf{n_q}). \tag{3}$$

Here

$$N_{\nu l} = (-1)^{(\nu-l)/2}\sqrt{\frac{2\Gamma[(\nu-l+2)/2]}{r_0^3\Gamma[(\nu+l+3)/2]}} \tag{4}$$

is the normalization of the oscillator functions, $\bar{q} = q/r_0$ is the dimensionless spatial coordinate, r_0 is the oscillator radius, Γ is the gamma function, $L_n^{(\beta)}$ is the generalized Laguerre polynomial, Y_{lm} is the spherical harmonic, l and m are the orbital angular momentum and its projection, and ν is the number of oscillator quanta. As a result, the total wave function (1) can be represented in the form of an expansion,

$$\Psi = \sum_{J=J_0}^{\infty}\sum_{M=-J}^{J}\sum_{s=|s_1-s_2|}^{s_1+s_2}\sum_{l=|J-s|}^{J+s}\sum_{\nu=\nu_0}^{\infty}C_{J^\pi Mls\nu}\,\Psi_{J^\pi Mls\nu}, \tag{5}$$

over basis functions,

$$\Psi_{J^\pi Mls\nu} = N_{J^\pi ls\nu}\,\mathcal{A}\left\{\sum_{m+\sigma=M}C_{lm\,s\sigma}^{JM}\left[\phi_{s_1}^{(1)}\phi_{s_2}^{(2)}\right]_{s\sigma}f_{\nu lm}(\mathbf{q})\right\}, \tag{6}$$

where the cluster spins s_1 and s_2 are coupled to the channel spin s (with the projection σ), which is, in turn, coupled with the orbital angular momentum l to the total angular momentum J (with the projection M), $C_{lm\,s\sigma}^{JM}$ is the Clebsch-Gordan coefficient, $N_{J^\pi ls\nu}$ is the normalization of the basis functions (6), π is the parity of the system, and ν_0 is the minimum number of oscillator quanta allowed by the Pauli exclusion principle.

Thus, the problem transforms to determination of the unknown expansion coefficients $C_{J^\pi Mls\nu}$. In the general case, these coefficients obey an infinite set of linear algebraic equations,

$$\begin{cases}\displaystyle\sum_{s=|s_1-s_2|}^{s_1+s_2}\sum_{l=|J-s|}^{J+s}\sum_{\nu=\nu_0}^{\infty}\left(\langle J^\pi M\tilde{l}\tilde{s}\tilde{\nu}|H|J^\pi Mls\nu\rangle - E\,\delta_{\tilde{s}s}\delta_{\tilde{l}l}\delta_{\tilde{\nu}\nu}\right)C_{J^\pi Mls\nu} = 0, \\[6pt] \tilde{s} = |s_1-s_2|,\ldots,s_1+s_2, \quad \tilde{l} = |J-\tilde{s}|,\ldots,J+\tilde{s}, \quad \tilde{\nu} = \nu_0, \nu_0+2,\ldots,\end{cases} \tag{7}$$

obtained by projecting the multiparticle Schrödinger equation for the total wave function (5) onto the basis functions (6),

$$\langle\Psi_{J^\pi Mls\nu}|H-E|\Psi\rangle = 0. \tag{8}$$

Here δ_{ij} is the Kronecker symbol, E is the total energy in the center-of-mass frame, and H is the translationally invariant microscopic Hamiltonian for the A-nucleon system,

$$H = T - T_{\text{c.m.}} + V_{\text{Coul}} + V_{\text{nucl}}, \tag{9}$$

where

$$T - T_{\text{c.m.}} = -\frac{\hbar^2}{2mA}\sum_{i>j=1}^{A}(\nabla_i - \nabla_j)^2 \tag{10}$$

is the kinetic energy,

$$V_{\text{Coul}} = \sum_{i>j=1}^{A}\frac{e^2}{|\mathbf{r}_i-\mathbf{r}_j|}\left(\frac{1}{2}-t_{3,i}\right)\left(\frac{1}{2}-t_{3,j}\right) \tag{11}$$

is the Coulomb interaction of the protons,

$$V_{\text{nucl}} = \sum_{i>j=1}^{A}V_{ij}^{(\text{nucl})} \tag{12}$$

is the nuclear interaction, and $V_{ij}^{(\text{nucl})}$ is a NN potential. In Eq. (10), ∇ is the nabla, m is the nucleon mass, and $\hbar$ is the Planck constant. In Eq. (11), $\mathbf{r}_i$ and $t_{3,i}$ are the radius vector and the isospin projection operator of the ith nucleon, and e is the elementary charge ($e > 0$).

The total angular momentum and parity conservation removes the summation over J and π in Eq. (7). Taking into account the boundary conditions for the discrete spectrum and the continuum of the considered nuclear system, the infinite set of Eqs. (7) can be reduced to the specific finite sets [13]. The solving a finite set of linear algebraic equations is not so difficult problem from the mathematical viewpoint. The most complicated task for realization of such a technique is to calculate the Hamiltonian matrix elements, which serve as coefficients of the corresponding sets of algebraic equations. A complexity originates from the need of the antisymmetrization

of the total wave function with respect to every pair permutation of the nucleons. This leads to a great number of terms in bra and ket vectors of the matrix elements. Nevertheless, there is a graceful procedure for avoiding these computational problems. It is based on the generating functions method [13]. The main idea of the method is to utilize the generating function,

$$\exp\left(-q^2/2r_0^2 + \mathbf{q}\mathbf{R}/r_0 - R^2/4\right)$$
$$= \sum_{vlm} B_{vl} f_{vlm}(\mathbf{q}) \frac{R^v}{v!} Y_{lm}^*(\mathbf{n_R}), \qquad (13)$$

for the oscillator functions (3). In Eq. (13), $\mathbf{R}$ is the generating parameter, and the coefficients B_{vl} are expressed by

$$B_{vl} = \frac{(\pi r_0)^{3/2} \, v!}{2^{v-1/2}\sqrt{\Gamma[(v-l+2)/2]\,\Gamma[(v+l+3)/2]}}. \qquad (14)$$

Replacing f_{vlm} in Eq. (6) by the left-hand side of relation (13), one can obtain the generating functions for the basis functions (6). The use of the generating functions simplifies the calculation of matrix elements. Having calculated the generating matrix elements $\langle \mathbf{Q}, s_f\sigma_f | V | \mathbf{R}, s_i\sigma_i \rangle$ for an arbitrary operator V, all its matrix elements $\langle J_f^{\pi_f} M_f l_f s_f v_f | V | J_i^{\pi_i} M_i l_i s_i v_i \rangle$ between the basis functions (6) can be deduced from the relation,

$$\langle J_f^{\pi_f} M_f l_f s_f v_f | V | J_i^{\pi_i} M_i l_i s_i v_i \rangle$$

$$= \frac{1}{\kappa_{v_f l_f s_f} \kappa_{v_i l_i s_i} v_f! v_i!} \left[\frac{\partial^{v_f}}{\partial Q^{v_f}} \frac{\partial^{v_i}}{\partial R^{v_i}} \sum_{\substack{m_f+\sigma_f=M_f, \\ m_i+\sigma_i=M_i}} C_{l_f m_f \, s_f \sigma_f}^{J_f M_f} C_{l_i m_i \, s_i \sigma_i}^{J_i M_i} \iint Y_{l_f m_f}^*(\mathbf{n_Q}) \langle \mathbf{Q}, s_f\sigma_f | V | \mathbf{R}, s_i\sigma_i \rangle Y_{l_i m_i}(\mathbf{n_R}) d\mathbf{n_Q} d\mathbf{n_R} \right]_{Q=R=0}, \qquad (15)$$

with

$$\kappa_{vls}^2 = \frac{2\pi}{(v!)^2} \left[\frac{\partial^v}{\partial Q^v} \frac{\partial^v}{\partial R^v} \int_{-1}^1 \langle \mathbf{Q}, s\sigma | \mathbf{R}, s\sigma \rangle P_l(t) dt \right]_{Q=R=0}, \qquad (16)$$

where $P_l(t)$ is the Legendre polynomial, and t is the cosine of the angle between vectors $\mathbf{Q}$ and $\mathbf{R}$. Expression (16) comes from the basis orthonormality.

The ^{6}Li nucleus is a weakly bound stable one. It has the single bound state with the total energy $E_{g.s.} = -31.994$ MeV and with the total angular momentum and the parity $J^\pi = 1^+$. This state breaks into an α particle and a deuteron at the excitation energy $\varepsilon = 1.474$ MeV (the breakup threshold). In the present paper, this state is described as the bound one of the α and d clusters that contain the protons and the neutrons in the lowest harmonic-oscillator shells. It assumes that the intrinsic cluster wave functions are given in the form of the translationally invariant oscillator shell-model wave functions for the lowest states compatible with the Pauli exclusion principle. The α-d relative motion wave function is expanded in series of the oscillator functions. The channel spin s is equal to 1 ($s_\alpha = 0$; $s_d = 1$), and the orbital angular momentum l is equal to 0 and 2 in accordance with the composition of moments and the parity conservation. In the framework of the approach, the ^{6}Li total wave function is found by the solving set (7) written for the discrete spectrum [13].

The total wave functions for the ^{4}He + ^{2}H scattering states follow from the solving set (7) written for the continuum [13]. Here the α and d clusters are also supposed to occupy the lowest configurations of the translationally invariant oscillator shell model and to have the channel spin $s = 1$ as in the previous case of the α-d discrete spectrum. The orbital angular momentum can take one or two values depending on J^π. For example, l is equal to 1 for states with $J^\pi = 0^-$ and 1^- and

$l = 2$ for $J^\pi = 2^+$. In turn, l is equal to 0 and 2 for $J^\pi = 1^+$, $l = 1$ and 3 for $J^\pi = 2^-$, $l = 2$ and 4 for $J^\pi = 3^+$, and so on.

In order to solve the set of Eqs. (7) for the discrete spectrum and for the continuum of the α-d system, the Hamiltonian matrix elements in the basis (6) should be calculated. The generating matrix elements necessary for this aim are presented in Appendix A.

Values of the oscillator radius r_0 for the intrinsic cluster wave functions and for the oscillator basis are supposed to be the same in Eq. (6). A choice of the oscillator-radius value allows one to correct an approximate description of the internal cluster states. The relative motion is not affected by this choice because the convergence of the expansion can be achieved with a required precision. It is worth noting that calculations of observables for the α-d continuum (for example, the nuclear phase shifts) should be performed at a significantly larger basis size than calculations for the α-d discrete spectrum (in particular, the ^{6}Li ground-state properties). At the same time, the calculations of the α-d radiative-capture cross section, which is determined by the overlap of the continuum and discrete-spectrum states, require the correct allowance for the tail of the ^{6}Li ground-state wave function at long enough distances. As a result, many terms of the expansion of this function over the basis (6) must be retained. This is a consequence of the peripheral character of the α-d radiative-capture process at low energies. The number of the basis functions used in the present paper is sufficient to achieve the good convergence of the results in all considered cases. For each state with the fixed J^π, M, l, and s values, 500 basis functions (6) are, at least, utilized. The elaborated well numerical procedures and algorithms of the implemented approach make it possible to use even larger sizes of the basis, but there is no a need to do that. Practically, the reliable results for the α-d system can be obtained at lower sizes of the truncated basis.

The nuclear interaction in the considered system is described by the realistic effective *NN* potential taken from work [71]. The general form of this potential, which consists of the central, spin-orbit, and tensor forces, is defined in Appendix A. The central and tensor components have three-range Gaussian forms, and the spin-orbit one has a two-range Gaussian form. It was shown in numerous works (see, for example, Refs. [13,14,71–73]) that the potential of such a type was a rather good approximation for a description of the nuclear interaction in microscopic studies of structure of light nuclei and dynamics of light-nucleus-induced reactions.

III. ELECTROMAGNETIC MULTIPOLE OPERATORS

At the leading order of the long-wavelength limit, the electric and magnetic multipole operators in the translationally invariant form can be written as

$$M_{I\mu}^{\rm E} = e \sum_{j=1}^{A} g_l(j) \, \bar{r}_j^I Y_{I\mu}(\mathbf{n}_{\bar{\mathbf{r}}_j}), \tag{17}$$

$$M_{I\mu}^{\rm M} = \mu_{\rm N} \sum_{j=1}^{A} \left(g_s(j)\,\mathbf{s}_j + \frac{2g_l(j)}{I+1}\,\bar{\mathbf{L}}_j \right) \left[\nabla_{\bar{\mathbf{r}}_j} \bar{r}_j^I Y_{I\mu}(\mathbf{n}_{\bar{\mathbf{r}}_j}) \right], \tag{18}$$

where the following denotations are introduced:

$$\bar{\mathbf{L}}_j = \bar{\mathbf{r}}_j \times \bar{\mathbf{p}}_j, \tag{19}$$

$$\bar{\mathbf{r}}_j = \mathbf{r}_j - \mathbf{r}_{\rm c.m.}, \tag{20}$$

$$\bar{\mathbf{p}}_j = \mathbf{p}_j - \frac{\mathbf{p}_{\rm c.m.}}{A}, \tag{21}$$

$$g_l(j) = \frac{1}{2} - t_{3,j}, \tag{22}$$

$$g_s(j) = \frac{1}{2}(g_{\rm n} + g_{\rm p}) + t_{3,j}\,(g_{\rm n} - g_{\rm p}), \tag{23}$$

$\mathbf{p}$ and $\mathbf{s}$ are the momentum and the spin of a nucleon, $\mathbf{r}_{\rm c.m.}$ and $\mathbf{p}_{\rm c.m.}$ are the radius vector and the momentum of the center-of-mass, I and μ are the multipolarity and its projection, $g_{\rm n}$ and $g_{\rm p}$ are the neutron and proton gyromagnetic factors, and $\mu_{\rm N}$ is the nuclear magneton.

Expression (17) for $I = 1$ read

$$M_{1\mu}^{\rm E} = e \sum_{j=1}^{A} g_l(j) \bar{r}_j Y_{1\mu}(\mathbf{n}_{\bar{\mathbf{r}}_j}). \tag{24}$$

The E1 operator defined by Eq. (24) is specific. Its isoscalar component vanishes,

$$\frac{e}{2} \sum_{j=1}^{A} \bar{r}_j Y_{1\mu}(\mathbf{n}_{\bar{\mathbf{r}}_j}) = 0, \tag{25}$$

and the isovector one,

$$-e \sum_{j=1}^{A} t_{3,j}\, \bar{r}_j Y_{1\mu}(\mathbf{n}_{\bar{\mathbf{r}}_j}), \tag{26}$$

remains only. The latter also vanishes for transitions between states with the total isospin $T = 0$. These are the isospin-forbidden E1 transitions.

At the first order beyond the leading order of the long-wavelength approximation (FOLWA), the E1 operator has a nonzero isoscalar part, which consists of three components [74],

$$M_{1\mu}^{\rm E(FOLWA)} = \tilde{M}_{1\mu}^{\rm E(1)} + \tilde{M}_{1\mu}^{\rm E(2)} + \tilde{M}_{1\mu}^{\rm E(3)}$$

$$= -\frac{ek_\gamma^2}{60} \sum_{j=1}^{A} \bar{r}_j^3 Y_{1\mu}(\mathbf{n}_{\bar{\mathbf{r}}_j})$$

$$+ \frac{\mu_{\rm N} k_\gamma}{4} \sum_{j=1}^{A} \bar{r}_j \left[\bar{\mathbf{L}}_j\, Y_{1\mu}(\mathbf{n}_{\bar{\mathbf{r}}_j}) \right]$$

$$\cdot \left(\frac{2}{3}\bar{\mathbf{L}}_j + (g_{\rm n} + g_{\rm p})\,\mathbf{s}_j \right), \tag{27}$$

where $k_\gamma = E_\gamma/\hbar c$ is the photon wave number, and E_γ is the energy of the emitted photon. A general expression for the electric multipole operator at this order of the approximation at an arbitrary value of the multipolarity I can be also found in Ref. [74].

For the two-cluster system, the E1 operator (24) at the leading order of the long-wavelength limit can be expressed by

$$M_{1\mu}^{\rm E} = M_{1\mu}^{\rm E(1)} + M_{1\mu}^{\rm E(2)} + e \frac{Z_1 A_2 - Z_2 A_1}{A_1 + A_2} \rho Y_{1\mu}(\mathbf{n}_\rho), \tag{28}$$

where $M_{1\mu}^{\rm E(1)}$ and $M_{1\mu}^{\rm E(2)}$ are the E1 operators defined by Eq. (24) for the clusters with the mass and charge numbers (A_1, Z_1) and (A_2, Z_2), and $\rho = \mathbf{r}_{\rm c.m.}^{(1)} - \mathbf{r}_{\rm c.m.}^{(2)}$ is the relative vector between the cluster centers of mass. Expression (28) is equivalent to Eq. (24). Both of them are equal to zero for E1 transitions between zero-isospin states in self-conjugate systems. Nevertheless, if one uses the measured values of the cluster masses m_1 and m_2 instead of $m_1 = A_1 m$ and $m_2 = A_2 m$, which follow from the isospin formalism, one can rewrite Eq. (28) in an alternative form that connects the respective transitions:

$$M_{1\mu}^{\rm E(PEM)} = e \frac{Z_1 m_2 - Z_2 m_1}{m_1 + m_2} \rho Y_{1\mu}(\mathbf{n}_\rho). \tag{29}$$

The replacement of the cluster masses from the isospin formalism by their values extracted from experiment is known as the PEM. In most works cited in the Introduction, the PEM was exploited to take into consideration the isospin-forbidden E1 transitions for the ^{2}H$(\alpha, \gamma)^6$Li reaction. At the same time, the PEM was criticized in the recent work [46]. The main reason is a lack of a microscopic justification.

In the present paper, the E2 and M1 transitions are calculated at the leading order of the long-wavelength limit. The isospin-forbidden E1 transitions are examined at the FOLWA, utilizing Eq. (27). The PEM based on Eq. (29) is also used to make the picture complete. Actually, there is an alternative way. Particularly, one can include isospin admixtures in the wave functions and apply Eq. (26) in the calculations. However, the last point is beyond the scope of the paper.

Expressions for the generating matrix elements of the E1, E2, and M1 operators together with their reduced matrix elements between the basis functions (6) for the α-d system are given in Appendix B. The reduced matrix elements of these operators are required to calculate the electromagnetic moments for the ^{6}Li ground state and the total cross section (the astrophysical S factor) for the α-d radiative capture.

The electric quadrupole and magnetic dipole moments of the ^{6}Li ground state in the framework of the approach, respectively, read

$$Q = \frac{2}{5}\sqrt{\frac{2\pi}{3}} \sum_{\tilde{l},\,l=0,\,2} \sum_{\tilde{\nu},\,\nu=\nu_0}^{\nu_{\max}} C^{(\mathrm{DS})}_{1^+\tilde{l}s\tilde{\nu}} \langle 1^+\tilde{l}s\tilde{\nu}\|M_2^{\mathrm{E}}\|1^+ls\nu\rangle C^{(\mathrm{DS})}_{1^+ls\nu}, \tag{30}$$

$$\mu = \frac{\sqrt{2\pi}}{3} \sum_{l=0,\,2} \sum_{\tilde{\nu},\,\nu=\nu_0}^{\nu_{\max}} C^{(\mathrm{DS})}_{1^+ls\tilde{\nu}} \langle 1^+ls\tilde{\nu}\|M_1^{\mathrm{M}}\|1^+ls\nu\rangle C^{(\mathrm{DS})}_{1^+ls\nu}, \tag{31}$$

where $C^{(\mathrm{DS})}_{1^+ls\nu}$ are the expansion coefficients of the ^{6}Li ground-state wave function over the basis (6), and $\nu_{\max}$ is the maximum number of oscillator quanta for the truncated basis. Note that the reduced matrix elements of the E2 operator in Eq. (30) are exactly zero for $\tilde{l} = l = 0$.

The partial cross section for the ^{2}H$(\alpha, \gamma)^6$Li radiative capture reaction within the approach have the form

$$\sigma_{(J_i^{\pi_i},\,l_i)\,\to\,1^+}(E_{\mathrm{c.m.}}, \Lambda I) = \frac{8\pi(I+1)}{3(2l_i+1)\hbar I[(2I+1)!!]^2}\left(\frac{E_\gamma}{\hbar c}\right)^{2I+1}\left|\sum_{l_f=0,\,2}\sum_{\nu_f=\nu_0}^{\nu_{\max}}\sum_{\nu_i=\nu_0}^{\nu'_{\max}} C^{(\mathrm{DS})}_{1^+l_fs\nu_f}\langle 1^+l_fs\nu_f\|M_I^\Lambda\|J_i^{\pi_i}l_is\nu_i\rangle C^{(\mathrm{CS})}_{J_i^{\pi_i}l_is\nu_i}\right|^2. \tag{32}$$

Here $E_{\mathrm{c.m.}}$ is the relative motion energy of the colliding nuclei in the center-of-mass system, and $C^{(\mathrm{CS})}_{J_i^{\pi_i}l_is\nu_i}$ are the expansion coefficients of the total wave functions for the α-d scattering states over the basis (6). The initial quantum numbers $(J_i^{\pi_i}, l_i)$ can take the values of

$$(0^-,\,1),\,(1^-,\,1),\,(2^-,\,1),\,\text{and}\,(2^-,\,3)\,\text{for the E1 captures}, \tag{33}$$

$$(1^+,\,0),\,(1^+,\,2),\,(2^+,\,2),\,(3^+,\,2),\,\text{and}\,(3^+,\,4)\,\text{for the E2 captures}, \tag{34}$$

$$(1^+,\,0),\,(1^+,\,2),\,\text{and}\,(2^+,\,2)\,\text{for the M1 captures}. \tag{35}$$

The E1 and E2 transitions to the S ($l_f = 0$) and D ($l_f = 2$) waves of the ^{6}Li ground state come from all P-scattering ($l_i = 1$) and D-scattering ($l_i = 2$) states presented in Eqs. (33) and (34), respectively. The E1 transition from the F-scattering state ($l_i = 3$) and the E2 transitions from the S-scattering ($l_i = 0$) and G-scattering ($l_i = 4$) states are only possible to the D-wave bound state. As to the M1 transitions, they occur between S states and between D states of the initial and final channels. The sum of the partial cross sections expressed by Eq. (32) for all allowed transitions gives the total cross section of the considered reaction.

At sub-barrier energies, a cross section of a reaction induced by charged particles rapidly falls with the relative motion energy decreasing. This strong dependence is predominantly caused by the penetrability of the Coulomb barrier. That is why it is generally accepted to write the cross section of a charged-particle-induced reaction in terms of the astrophysical S factor,

$$\sigma(E_{\mathrm{c.m.}}) = \frac{\exp\left(-\sqrt{E_{\mathrm{G}}/E_{\mathrm{c.m.}}}\right)}{E_{\mathrm{c.m.}}}\,S(E_{\mathrm{c.m.}}), \tag{36}$$

where E_{G} is the Gamow energy for the colliding particles. In fact, Eq. (36) implicitly defines the astrophysical S factor for the reaction. The astrophysical S factor has smoother energy behavior than the cross section because the exponentially small factor of the Coulomb barrier penetrability is explicitly extracted from it. The partial astrophysical S factors for the α-d radiative capture are related to the corresponding partial cross sections (32) by Eq. (36), in which the Gamow energy E_{G} is about equal to 5.258 MeV for the α-d system.

IV. RESULTS AND DISCUSSION

A. Potential parametrizations

In the present paper, different parametrizations hereinafter referred to as MHN2, NHN2, and PHN are used for the adopted nuclear potential. They generalize parametrizations introduced in works [71,72] and referred to as NHN and MHN. The MHN and the NHN differ from each other by the short-range part of the central force. Changes only of the long-range part of the tensor force in the MHN and the NHN lead to the MHN2 and the NHN2, respectively. Changing the long-range part of the tensor force and the short-range part of the central one gives the PHN. The differences between the parametrizations are explicitly demonstrated in Appendix A.

The intensity of the central Majorana force (g_c) and the intensities of the spin-orbit (g_{ls}) and tensor (g_t) interactions chosen in the calculations are given in Table I. In order to explore an effect of the potential on the calculated observables, various sets of values of the intensities are applied. For this

MICROSCOPIC DESCRIPTION OF THE ^{2}H(α, γ)^{6}Li ...

PHYSICAL REVIEW C **106**, 014610 (2022)

TABLE I. The parametrizations of the nuclear potential and oscillator-radius values (in femtometers) used in the calculations.

Abbreviation	g_c	g_{ls}	g_t	r_0
MHN2-I	0.988	21.944	1.036	1.45
MHN2-II	0.982	28.720	1.066	1.55
NHN2-I	0.953	23.438	1.051	1.45
NHN2-II	0.948	29.962	1.076	1.55
PHN-I	0.992	23.320	1.020	1.22
PHN-II	0.978	30.900	0.936	1.35
PHN-III	0.966	49.343	0.983	1.55

reason, the abbreviations of the potential parametrizations are supplied with Roman numerals. Values of the oscillator radius r_0 are also presented in Table I.

B. Nuclear spectroscopy and electromagnetic properties of the ^{6}Li nucleus

In the framework of the approach, the following ground-state observables of ^{6}Li are calculated: the ground-state energy ($E_{g.s.}$), the point-proton rms radius (r_p), the electric quadrupole moment (Q), the magnetic dipole moment (μ), the breakup threshold into α and d (ε), and the binding energies of the α (E_α) and d (E_d) clusters. The results are summarized in Table II. Experimental values of these quantities from works [75–79] are collected in Table III.

As can be seen from Tables II and III, the α and d clusters as well as the ^{6}Li nucleus turn out to be underbound in the MHN2 and NHN2 calculations. Here the point-proton rms radius of ^{6}Li is slightly overestimated. The calculation with the PHN-I reproduces the α, d, and ^{6}Li energies whereas r_p is underestimated. This radius is reproduced in the PHN-II calculation but the considered clusters and ^{6}Li are overbound. In all cases, the breakup threshold of ^{6}Li into the clusters and the tiny magnitude of the ^{6}Li electric quadrupole moment, including its sign, are reproduced, and the magnetic dipole moment is slightly overestimated. The nonzero value of Q within the approach is generated by the tensor force through the D state of ^{6}Li.

Evidently, it is very difficult to reproduce all available experimental data of different kinds on the considered six-nucleon system, using a rather restricted model space within

TABLE III. The ^{6}Li observables from experiments [75–79]. The units of measure are those as in Table II.

E_α	E_d	$E_{g.s.}$	ε	r_p	Q	μ
28.296	2.224	−31.994	1.474	2.38(3)	−0.0818(16)	0.822

the approach. Although, the most suitable potential for achieving this aim for data from Table III is the PHN-I.

The calculated energies (E_r) of ^{6}Li low-lying resonances with the total isospin $T = 0$ are compared with experimental data [77] in Table IV. The energy of the lowest 3^+ resonance is reproduced. As to the energies of the 2^+ and 1^+ resonances, they are slightly underestimated in the case of the MHN2 and the NHN2 but overestimated for the PHN. The splitting between the 2^+ and 1^+ resonances, especially for the PHN calculation, is close enough to the experimental one. The positions of the 2^+ and 1^+ resonances govern the resonance behavior of the respective α-d D-wave nuclear phase shifts, which do not affect the α-d radiative capture at astrophysical energies. Keeping in mind this fact, one can state that the deviation of these calculated resonance positions from the experiment is not so important in regard to the main goal of the present paper focused on a microscopic low-energy description of the α-d radiative-capture reaction.

C. ANCs for the bound S and D states of ^{6}Li in the $\alpha + d$ channel. Deformation effects

The tail of the ^{6}Li S-wave function in the $\alpha + d$ channel is known [31–33] to give an important contribution to the low-energy behavior of the $\alpha + d$ radiative capture reaction due to the peripheral nature of the process. The amplitude of the tail is the ANC for the bound S state of ^{6}Li in the $\alpha + d$ channel (C_0). Thus, this quantity plays a significant role for the $\alpha + d$ radiative capture at astrophysical energies. The ^{6}Li S-state ANCs extracted from analyses of experimental data are given in Table V where the following abbreviations are introduced: FDRA is a forward dispersion relation analysis of d-α elastic-scattering data [80], ATAP1 is an analysis of data on the tensor analyzing powers (TAPs) for the ^{6}Li($\vec{d}, \alpha$)^{4}He reaction [81], ACPA is an analytic continuation of the solution of an energy-dependent phase-shift analysis of elastic d-α

TABLE II. The ^{6}Li calculated properties.

Quantity	MHN2-I	MHN2-II	NHN2-I	NHN2-II	PHN-I	PHN-II	PHN-III
E_α (MeV)	27.384	25.369	27.355	25.344	28.296	29.291	25.843
E_d (MeV)	0.031	0.281	0.027	0.278	2.224	2.736	2.494
$E_{g.s.}$ (MeV)	−28.889	−27.124	−28.856	−27.096	−31.994	−33.501	−29.811
ε (MeV)	1.474	1.474	1.474	1.474	1.474	1.474	1.474
r_p (fm)	2.44	2.52	2.45	2.53	2.28	2.39	2.55
Q (e fm^2)	−0.0818	−0.0818	−0.0818	−0.0818	−0.0818	−0.0818	−0.0818
μ (μ_N)	0.87988	0.87989	0.87988	0.87989	0.87987	0.87988	0.87990
C_0 (fm$^{-1/2}$)	2.44	2.53	2.49	2.56	2.32	2.43	2.60
C_2 (fm$^{-1/2}$)	−0.0077	−0.008	−0.0077	−0.008	−0.0073	−0.0075	−0.008
η	−0.0032	−0.0032	−0.0031	−0.0031	−0.0031	−0.0031	−0.0031

TABLE IV. The calculated energies (in MeV) of the ^{6}Li low-lying resonances ($T = 0$) compared to the experiment [77].

Energy	MHN2-II	NHN2-II	PHN-I	Experiment
$E_r (3^+)$	0.712	0.712	0.712	0.712
$E_r (2^+)$	2.642	2.653	5.034	2.838
$E_r (1^+)$	3.705	3.694	6.548	4.176

scattering to the pole corresponding to the ^{6}Li ground state on the basis of the statistical Padé approximation [82], ATAP2 is an analysis of data on the TAP for ($\vec{^6\mathrm{Li}}, d$) reactions on medium-heavy targets [83], and PSA is a phase shift analysis of ^{6}Li + ^{4}He elastic scattering data [84]. The calculated C_0 values from Table II are close to the ACPA and PSA results. The C_0 value obtained with the PHN-I is in perfect agreement with those data.

The importance of nonspherical terms of light nuclei has been well understood many years ago [85,86]. Nevertheless, the problem of D-state manifestations in ^{6}Li still remains. In general, a question concerned with the magnitude of nonspherical components of the ^{6}Li ground-state total wave function is open. For example, the nonzero negative electric quadrupole moment Q of ^{6}Li points out the presence of these components and the tensor force. In this respect, a study of the D-state terms is also useful for understanding of the tensor components of the NN potential, which particularly generate these terms for S-shell nuclei. However, experimental obtaining information about nonspherical components for ^{6}Li is known to be very difficult [83,84,86].

Nuclear deformation effects in light nuclei could be quantified by the ratio of the D- and S-state ANCs ($\eta = C_2/C_0$) [86]. It characterizes the relative strength of the D-state term of the wave function in the asymptotic region where the influence of the nuclear interaction is negligible. An experimental determination of this quantity is possible [83,84,86]. In addition to nonzero Q for ^{6}Li, a nonzero value of η is another indication of a role of the D-state components in the ^{6}Li wave function. Obviously, information about η for ^{6}Li serves as an additional useful knowledge of its nuclear structure. Moreover, this information could have some practical applications [83]. However, η for ^{6}Li is known poorer than for other lighter nuclei [85,86]. In the case of ^{6}Li, there are yet no unambiguous results for the magnitude of η and even its sign. Values of the ANC C_2 for the bound D state of ^{6}Li in the $\alpha + d$ channel and the asymptotic D- to S-state ratio η for ^{6}Li from experiments are presented in Table V.

There are also works [87–90] (not presented in Table V) that provide additional findings on the magnitude of the ratio
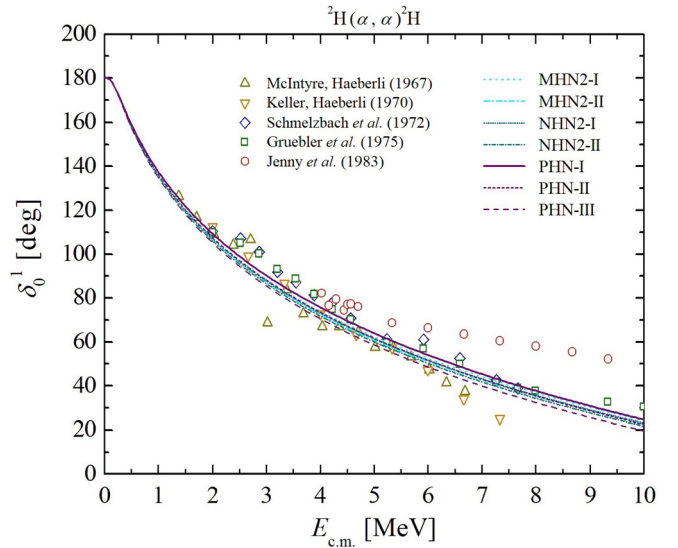

FIG. 1. The 1^+ S-wave nuclear phase shift for the ^{4}He + ^{2}H elastic scattering.

η and its sign based on experimental data analyses. Measurements of the TAP in the inclusive breakup of polarized $\vec{^6\mathrm{Li}}$ in Ref. [87] give data, which favor a small positive value of η. In an analysis of measured data on $\vec{^6\mathrm{Li}}$ + ^{58}Ni elastic scattering [88], it was summarized that the value of η must be small and negative. Based on a reanalysis of the data [88], it was found in Ref. [89] that the value of η should be very close to zero with the negative sign. In Ref. [90], using measured $\vec{^6\mathrm{Li}}$ + ^{4}He elastic-scattering data, it was concluded that the value of η was very small and could not be other than negative.

The calculations from Table II actually give $C_2 \approx$ $-0.008 \div -0.007$ fm$^{-1/2}$. These values are consistent well in the magnitude with the experimental result based on the FDRA. All calculations support a small negative value of the asymptotic D- to S-state ratio $\eta \approx -0.003$.

D. The ^{2}H(α, α)^{2}H elastic scattering

The calculated nuclear phase shifts δ_l^J for all partial S, P, and D waves of the α-d elastic scattering in a wide energy range are depicted in Figs. 1–7. Experimental data marked in these figures are taken from works [91–95]. It should be emphasized that the data have a scatter, and experimental errors are not presented. For these reasons, it is quite difficult to assess a degree of agreement between the theory and the experiment. Nevertheless, some statements concerning it are given.

TABLE V. The ^{6}Li ANCs (in fm$^{-1/2}$) and their ratio from experimental data.

Quantity	FDRA [80]	ATAP1 [81]	ACPA [82]	ATAP2 [83]	PSA [84]
C_0	1.69(4)		2.30(12)		2.28(7)
C_2	0.008(24)				−0.060(14)
η	0.0047[a]	−0.015 ÷ −0.010		0.0003(9)	−0.025(6)(10)

[a]Sign not determined.
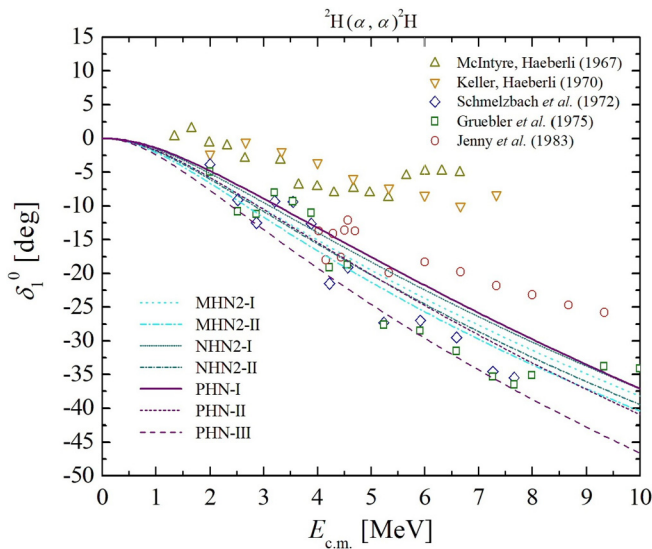
FIG. 2. The 0^- P-wave nuclear phase shift for the ^{4}He + ^{2}H elastic scattering.

FIG. 4. The 2^- P-wave nuclear phase shift for the ^{4}He + ^{2}H elastic scattering.

The calculated S-wave (δ_0^1) and D-wave (δ_2^3) nuclear phase shifts agree well with the data in Figs. 1 and 7, respectively. The calculated P-wave nuclear phase shifts δ_1^0, δ_1^1, and δ_1^2 in Figs. 2–4 demonstrate a monotonic decrease. The phase shift δ_1^0 is in agreement with the data whereas δ_1^1 and δ_1^2 deviate from the experimental points at high energies but remain close enough. The D-wave nuclear phase shifts δ_2^1 (Fig. 5) and δ_2^2 (Fig. 6) obtained with the MHN2 and the NHN2 describe the data reasonably. The calculations with the PHN give the underestimated phase shifts δ_2^1 and δ_2^2 because of the overestimated positions of the 1^+ and 2^+ resonances (see Table IV). However, the PHN yields the energy dependences of δ_2^1 and δ_2^2 similar to the experimental one.
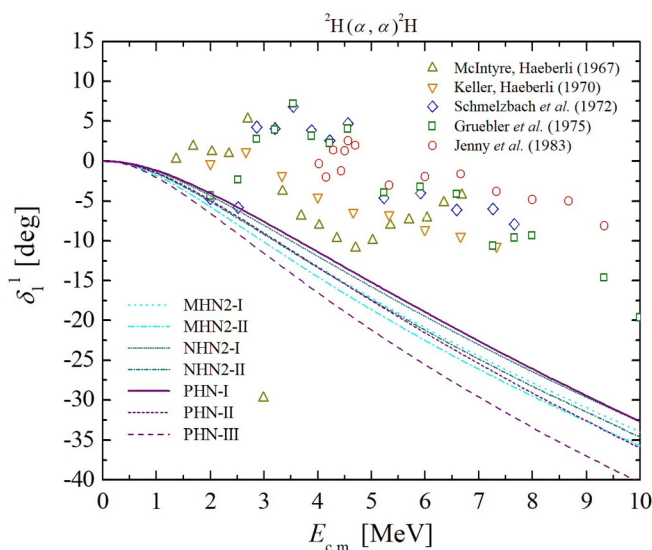
E. The ^{2}H(α, γ)^{6}Li radiative capture

In order to see the effect of choosing the different effective nuclear potentials on the resulting total astrophysical S factor of the ^{2}H(α, γ)^{6}Li reaction, the calculations are performed with the different parameterizations from Table I. The ^{2}H(α, γ)^{6}Li total astrophysical S factor calculated by using the PEM for the E1 operator is shown in Fig. 8. Experimental data [15–17,19,21,22] are drawn by symbols. All curves lie close to each other, reproduce the peak at 0.712 MeV from data [17], and agree reasonably with the other data in the considered energy range. The difference between the curves outside the vicinity of the peak is caused by two main reasons. At energies lower than the peak position, the reason is that the curves correspond to the different values of the ANC C_0

FIG. 3. The 1^- P-wave nuclear phase shift for the ^{4}He + ^{2}H elastic scattering.

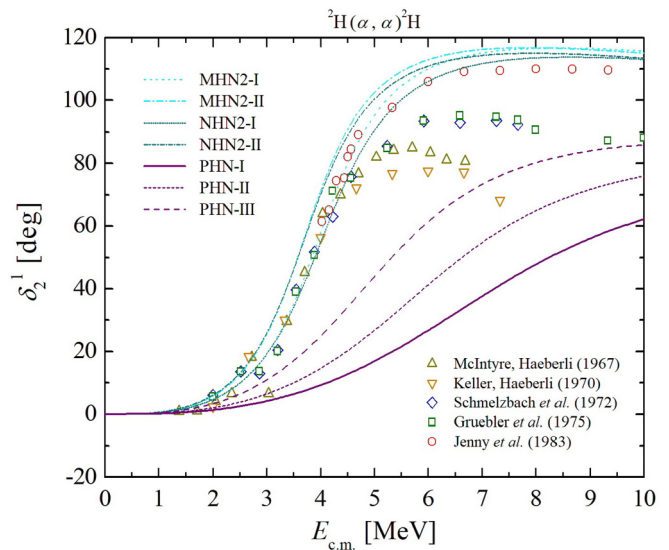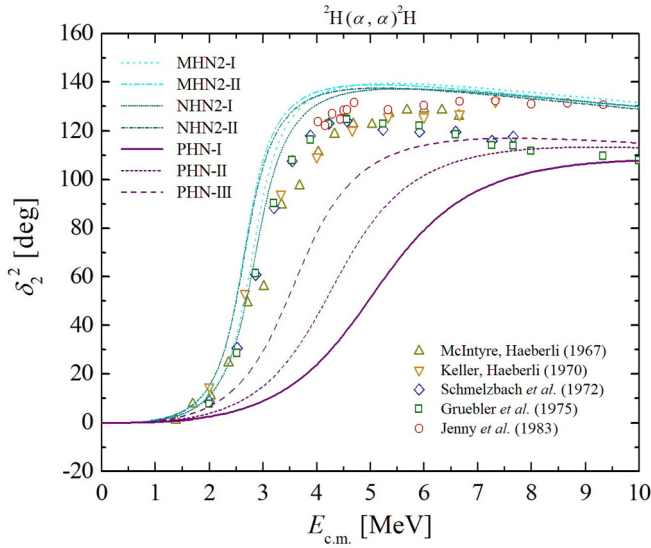FIG. 5. The 1^+ D-wave nuclear phase shift for the ^{4}He + ^{2}H elastic scattering.

FIG. 6. The 2^+ D-wave nuclear phase shift for the $^4\text{He} + {}^2\text{H}$ elastic scattering.

FIG. 8. The total astrophysical S factor for the $^2\text{H}(\alpha, \gamma){}^6\text{Li}$ reaction with the E1 transitions described by using the PEM.

playing a crucial role for the low-energy behavior of the peripheral process. At higher energies, it is a combined influence of the ANC and the 2^+ resonance, which is essentially closer to the 3^+ one for the MHN2 and NHN2 calculations than in the case of the PHN (see Table IV).

The $^2\text{H}(\alpha, \gamma){}^6\text{Li}$ total astrophysical S factor calculated with the E1 operator at the FOLWA is depicted in Fig. 9. The data outside the vicinity of the 3^+ peak, especially the modern data [19,21,22] at low energies, are described by the obtained curves better as compared with the previous ones in the PEM case. Explanations given above for the behavior of the curves in Fig. 8 also remain true for the curves in Fig. 9.

In order to arrive at a conclusion regarding which utilized potential to prefer and which astrophysical S-factor predic-
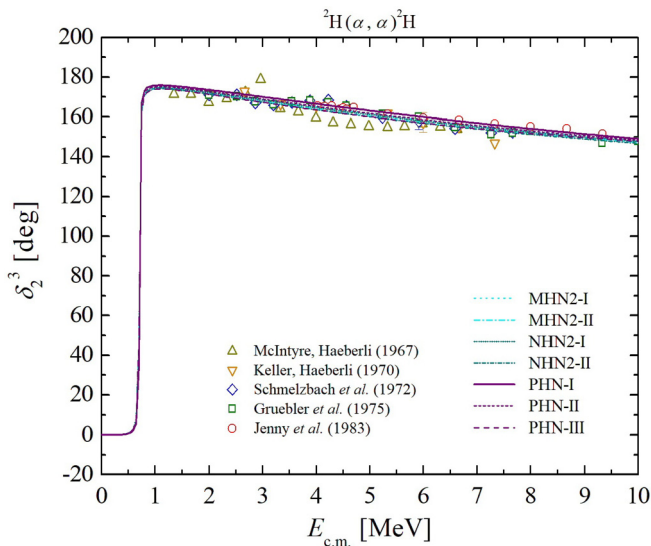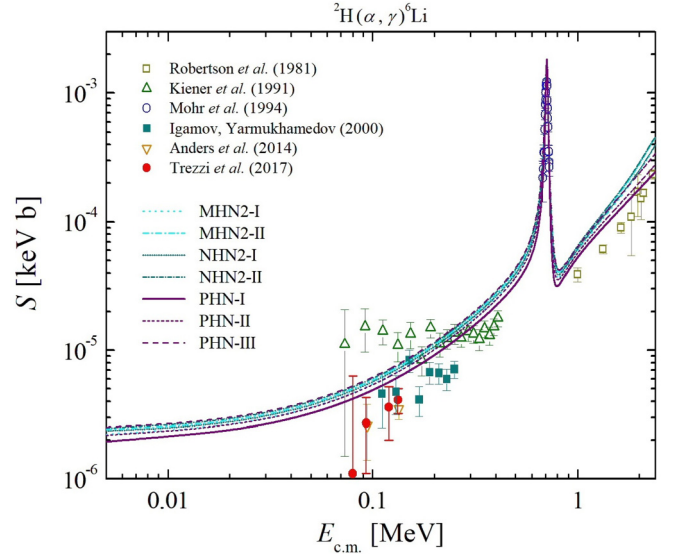
tion to adopt, first of all, one needs to have a look at the calculated nuclear properties of the considered six-nucleon system from Table II. It is clearly seen that the calculations with the PHN-I fit best the data from Tables III and V. Note that the calculated value obtained with this potential for the ^6Li S-state ANC playing a significant role for describing the α-d radiative capture at astrophysical energies [31–33] agrees perfectly with the ACPA [82] and PSA [84] results given in Table V. As for the nuclear phase shifts in Figs. 1–7, all potentials provide almost equivalent description of the 1^+ S- and 3^+ D-wave nuclear phase shifts. The P-wave nuclear phase shifts calculated with the PHN-I are closer to the data than the calculations with the other potentials. However, this potential results in the 1^+ and 2^+ D-wave nuclear phase

FIG. 7. The 3^+ D-wave nuclear phase shift for the $^4\text{He} + {}^2\text{H}$ elastic scattering.
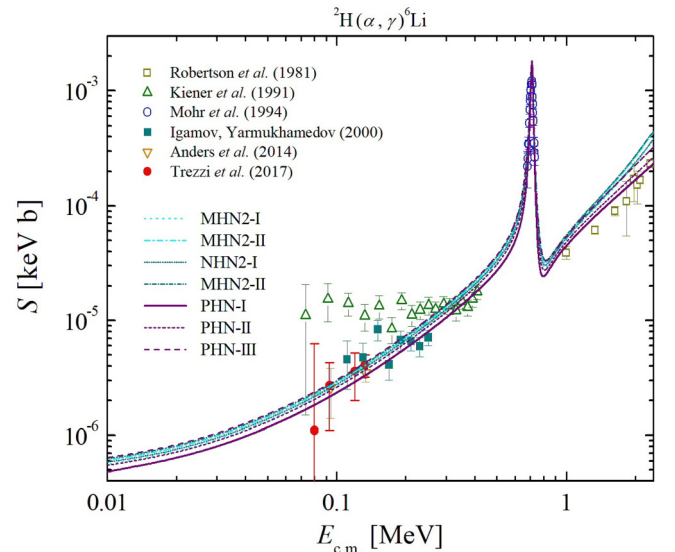

FIG. 9. The total astrophysical S factor for the $^2\text{H}(\alpha, \gamma){}^6\text{Li}$ reaction with the E1 transitions at the FOLWA.
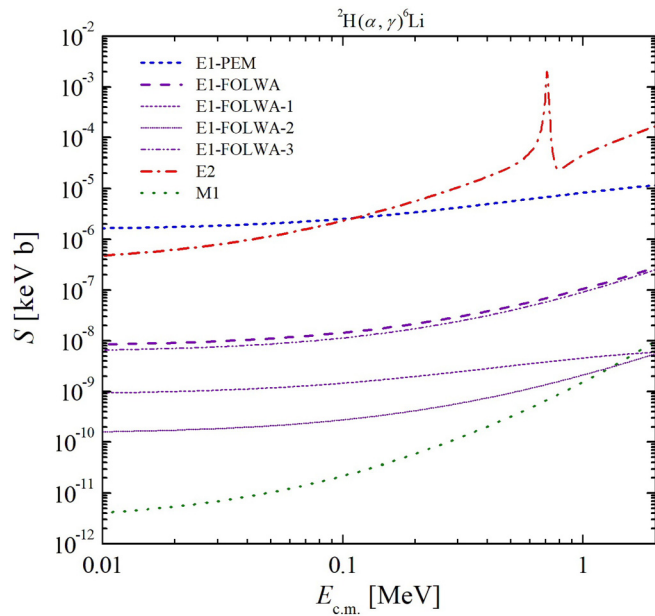
FIG. 10. The ^{2}H(α, γ)^{6}Li astrophysical S factors for the total E1, E2, and M1 captures calculated by using the PHN-I potential.
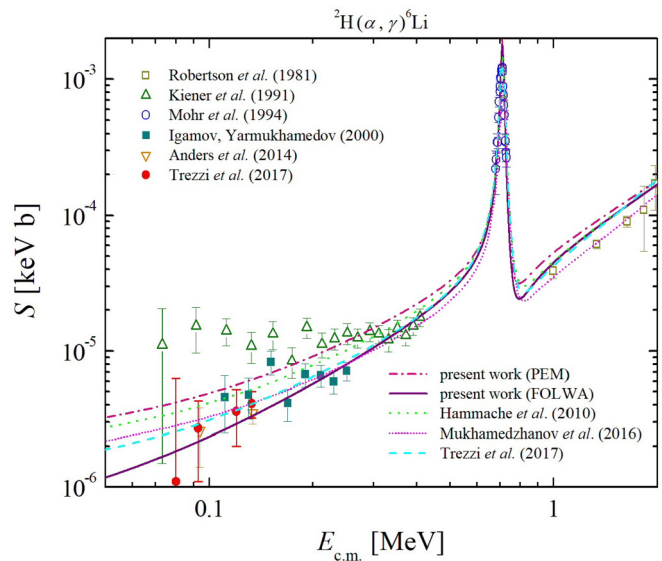

FIG. 11. Predictions from the present paper for the ^{2}H(α, γ)^{6}Li total astrophysical S factor calculated with the E1-PEM (dashed-dot line) and E1-FOLWA (full line) contributions compared to the results of the previous works [20,22,33].

shifts, which qualitatively show the resonance behavior but are underestimated quantitatively as compared to the data due to the overestimated positions of the 1^+ and 2^+ resonances presented in Table IV. Nevertheless, the indicated side effect does not affect the considered reaction at low energies. Thus, omitting this insignificant drawback that does not diminish the validity of the PHN-I, one can conclude that the PHN-I potential is overall better than the others used in the present paper for a self-consistent prediction from the implemented approach for the ^{2}H(α, γ)^{6}Li total astrophysical S factor at energies of astrophysical interest.

Obviously, the calculations in Fig. 8 differ from the calculations in Fig. 9 by the E1 contribution. The energy dependences of the E1, E2, and M1 capture contributions to the ^{2}H(α, γ)^{6}Li total astrophysical S factor calculated with the best PHN-I potential are plotted in Fig. 10.

The E1 contribution obtained with the PEM significantly exceeds the E1 one at the FOLWA and even lies higher than the E2 one at low energies (<110 keV). The E2 contribution is larger than the E1-FOLWA one in the whole energy region. The total M1 transition is essentially suppressed in comparison with the total E1-PEM, E1-FOLWA, and E2 ones at all considered energies. It means that the ^{2}H(α, γ)^{6}Li total astrophysical S factor is substantially formed by the E1-PEM and E2 contributions in Fig. 8 and only by the E2 one in Fig. 9. As to the E1-FOLWA contribution, it turns out to be small but not negligible one. The influence of the different components of the E1 operator (27) at FOLWA is also analyzed in Fig. 10. The E1-FOLWA contribution for the reaction is caused to a considerable degree by the third component of the E1 operator (27).

It should be noted that the total E1 capture for ^{2}H(α, γ)^{6}Li is mainly due to transitions from the P waves of the 0^-, 1^-, and 2^- scattering states to the 1^+ bound one. The F-wave E1 transition from the 2^- state is negligible. The D-wave transitions from the 1^+, 2^+, and 3^+ states are responsible for the total E2 capture as the S-wave transition from the 1^+ state is weak, and the G-wave one from the 3^+ state is strongly hindered. The total M1 capture is a result of the transitions from the D waves of the 1^+ and 2^+ states. The S-wave M1 transition from the 1^+ state is very weak.

Actually, the present microscopic calculation of the total astrophysical S factor based on the PEM for the E1 operator is only interesting to compare with the results of the previous PCM-based calculations exploiting the PEM and also estimate the magnitude of the PEM correction to the E1 transitions within the microscopic approach. In Fig. 11, the present predictions for the ^{2}H(α, γ)^{6}Li total astrophysical S factor obtained from the developed approach with the preferred PHN-I potential are compared with the predictions from works [20,33] (PCM, dotted and short dotted lines, respectively) and [22] (an analysis of the experimental data, dashed line). A comparison of the respective E1 and E2 contributions is demonstrated in Fig. 12.

As it can be seen in Fig. 11, the curves from the other works lie slightly lower than the PEM curve of the present paper, especially at energies below the resonance one. Despite this fact, the total astrophysical S factor calculated here with the E1-PEM contribution is rather similar to the results of the PCM-PEM-based works [20,33]. The result of Ref. [20] is the closest one to the present PEM curve. In turn, the E1-PEM and E2 contributions of the present paper in Fig. 12 are also the closest ones to the E1 and E2 contributions of Ref. [20], respectively. The obtained result for the E1-PEM contribution for lack of a rigorous microscopic justification for the PEM should be treated as estimation useful only for comparison with calculations from the PCM works where the PEM is widely used.
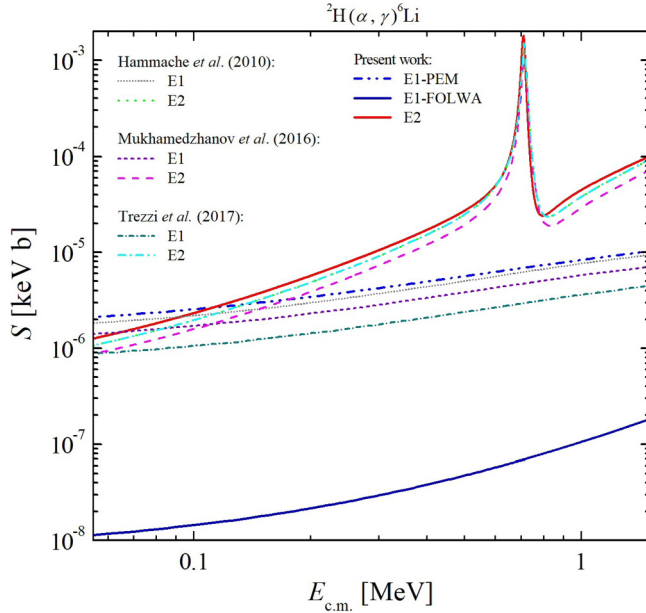
FIG. 12. Comparison of the E1 and E2 contributions to the energy dependence of the ^{2}H$(\alpha, \gamma)^6$Li total astrophysical S factor obtained in the different works.

The FOLWA prediction in Fig. 11 at energies above the resonance one almost coincides with the predictions from Refs. [20,22]. At lower energies, there is the difference due to mainly the E1 contribution. Excepting for the energies below about 300 keV, the ^{2}H$(\alpha, \gamma)^6$Li total astrophysical S factor calculated here with the E1-FOLWA contribution is quite similar to the result of Ref. [22] based on the analysis of the modern data. In that analysis, the E2 contribution is adopted from Ref. [20]. For this reason, the respective E2 curves are identical in Fig. 12. The E1 contribution in Ref. [22] is extracted by rescaling the E1 one of Ref. [20] so that the recommended total astrophysical S factor of Ref. [22] matches the data obtained in that work. Most likely, taking into account corrections to the isospin-forbidden E1 transitions caused by the isospin mixing in the wave functions within the developed approach is a possible way to smooth the indicated difference between the predictions from the present paper and work [22].

V. CONCLUSION

In the present paper, nuclear structure and dynamics of the six-nucleon ^{4}He + ^{2}H system have been studied microscopically, implementing the multichannel cluster approach formulated in the oscillator-basis representation and using the realistic effective nuclear potential. The different parametrizations of this potential have been applied to explore its influence on the obtained results. Moreover, such a procedure leads to the achievement of the optimum result. Clearly, the deuteron occupied the lowest harmonic-oscillator shell-model configuration is a quite simple approximation because the deuteron is an untight object as opposed to the α particle. That is why an appropriate choice of the nuclear potential form along with an oscillator-radius value is to some extent a

necessary condition of improving the model treatment of the studied system.

The α-d elastic scattering and the ^{6}Li ground-state properties have been considered. The energy dependences of the S-, P-, and D-wave nuclear phase shifts for the ^{2}H$(\alpha, \alpha)^2$H elastic scattering have been computed in the wide energy range. The most important 1^+ S- and 3^+ D-wave phase shifts agree well with the data from the experiments. That is true for the 0^- P-wave phase shift as well. The deviations inherent in the other phase shifts can be probably eliminated by taking into consideration the terms, such as so-called distortion effects, cluster rearrangements, pseudoinelastic configurations, and excited pseudostates, affecting the elastic scattering and the properties of the α-d system [48,49,96–99]. The energy and the electromagnetic observables of the ground state of the ^{6}Li nucleus as well as the energies of its low-lying resonance states with the zero total isospin have been calculated. The ^{6}Li ground-state asymptotic characteristics have been separately investigated. The ANCs for the bound S and D states of ^{6}Li in the $\alpha + d$ channel have been extracted. The deformation effects and the problem of the D-state manifestations in ^{6}Li have been also discussed. The present paper supports the small negative values of the asymptotic D- to S-state ratio. The best agreement with the experimental phase shifts and the ^{6}Li data important for a reliable treatment of the ^{2}H$(\alpha, \gamma)^6$Li reaction at astrophysical energies is achieved by exploiting the PHN-I potential in the calculations. In this regard, the PHN-I potential should be adopted as the preferred one to give a justified self-consistent prediction for the total astrophysical S factor of this reaction from the developed microscopic approach.

The most ambitious and intriguing problem studied here is the α-d radiative capture description. The ^{2}H$(\alpha, \gamma)^6$Li radiative-capture reaction has been considered at the astrophysically relevant energies, including the vicinity of the lowest 3^+ resonance of ^{6}Li. The energy dependence of the total astrophysical S factor has been thoroughly investigated. The isospin-forbidden E1 transitions have been treated by utilizing two different methods. The first one is based on the widely used PEM to give a complete picture. However, the result obtained with it should be interpreted as some estimation for lack of a rigorous microscopic justification for the PEM [46]. The second method making use of the FOLWA is fully justified from the microscopic viewpoint. The E1 contribution at the FOLWA turns out to be small but not negligible one as compared with the E2 contribution at the leading order of the long-wavelength limit. The M1 contribution is negligible. The E2 and M1 astrophysical S factors calculated with the PHN-I potential are the recommended ones within the approach. The recommended contribution of the E1 transitions through the isoscalar part of the E1 operator at FOLWA is also established with the PHN-I. The prediction for the resulting total astrophysical S factor obtained with this preferred potential yields the optimum result: the modern low-energy data [19,21,22] are described very well, the peak at 712 keV from the measurements [17] is reproduced, and there is the reasonable agreement with the data [15] at higher energies. Nevertheless, the corrections to the isospin-forbidden E1 transitions caused by the isospin admixtures in the wave functions, in particular, a small $T = 1$ isospin component of ^{6}Li, and the

isovector part of the E1 operator at the leading order of the long-wavelength limit should be also examined in the framework of the developed approach to come to the conclusive microscopic recommendation concerning the magnitude of the total E1 contribution. The effect of such corrections on the energy dependence of the total astrophysical S factor is still poorly known from the microscopic viewpoint.

Despite the smallness of the E1 transitions for the α-d system at the FOLWA, the respective method could be especially useful for other applications. Among them, for example, it is a microscopic description of the isospin-forbidden E1 transitions in the d-d system. In particular, the PEM does not work there at all.

The opportunities of the implemented approach have been shown to be rather promising to study the considered six-nucleon system. It has been also demonstrated that this approach is a well-grounded tool for the microscopic description of radiative capture reactions. Its further development should include enriching the model space by the terms mentioned above, which apparently affect nuclear structure and dynamics of the α-d system. The respective improvements are beyond the scope of the present paper. They must be investigated separately in the future.

ACKNOWLEDGMENT

APPENDIX A

The generating matrix elements required to calculate the Hamiltonian matrix for the six-nucleon ^{4}He $+ \, ^2$H system in the basis (6) are collected in this appendix.

The generating matrix elements for the unit operator read

$$\langle \mathbf{Q}, s\sigma_f | \mathbf{R}, s\sigma_i \rangle = \langle \mathbf{Q} | \mathbf{R} \rangle \delta_{\sigma_f \sigma_i}, \tag{A1}$$

where

$$\langle \mathbf{Q} | \mathbf{R} \rangle = \exp{(-\mathbf{Q}\mathbf{R}/3)}[\exp{(\mathbf{Q}\mathbf{R}/2)} - 1]^2. \tag{A2}$$

The generating matrix elements for the kinetic-energy operator (10) are expressed by

$$\langle \mathbf{Q}, s\sigma_f | T - T_{\text{c.m.}} | \mathbf{R}, s\sigma_i \rangle = \frac{\hbar^2}{12mr_0^2}\left(45 - 2\mathbf{Q}^2 - 2\mathbf{R}^2 + 6\,t\,\frac{\partial}{\partial t} \right) \langle \mathbf{Q} | \mathbf{R} \rangle \delta_{\sigma_f \sigma_i}. \tag{A3}$$

The generating matrix elements for the Coulomb potential (11) are given by

$$\langle \mathbf{Q}, s\sigma_f | V_{\text{Coul}} | \mathbf{R}, s\sigma_i \rangle$$

$$= \sqrt{\frac{2}{\pi}} \frac{e^2}{r_0} \langle \mathbf{Q} | \mathbf{R} \rangle \delta_{\sigma_f \sigma_i} \left\{ 1 + \frac{1}{\exp{(\mathbf{Q}\mathbf{R}/2)} - 1} \int_0^1 \left[2\,U^{(+)}(\varsigma, \mathbf{Q}, \mathbf{R}) - U^{(-)}(\varsigma, \mathbf{Q}, \mathbf{R}) - U^{(0)}(\varsigma, \mathbf{Q}, \mathbf{R}) \right] d\varsigma \right\}, \tag{A4}$$

where

$$U^{(+)}(\varsigma, \mathbf{Q}, \mathbf{R}) = \exp\left(-\frac{(\mathbf{Q}+\mathbf{R})^2}{8}\varsigma^2 + \frac{\mathbf{Q}\mathbf{R}}{2} \right), \tag{A5}$$

$$U^{(-)}(\varsigma, \mathbf{Q}, \mathbf{R}) = \exp\left(-\frac{(\mathbf{Q}-\mathbf{R})^2}{8}\varsigma^2 \right), \tag{A6}$$

$$U^{(0)}(\varsigma, \mathbf{Q}, \mathbf{R}) = \exp\left(-\frac{\mathbf{Q}^2}{8}\varsigma^2 \right) + \exp\left(-\frac{\mathbf{R}^2}{8}\varsigma^2 \right) - 1. \tag{A7}$$

The realistic effective nuclear potential adopted in the present paper to describe the nuclear interaction has the form

$$V_{\text{nucl}} = V_{\text{c}} + V_{ls} + V_{\text{t}}. \tag{A8}$$

It consists of the central (V_{c}), spin-orbit (V_{ls}), and tensor (V_{t}) forces [71], which can be defined by

$$V_{\text{c}} = \sum_{n=1}^{3} \sum_{i>j=1}^{A} V_{n,\,ij}^{(\text{c})}, \tag{A9}$$

$$V_{n,\,ij}^{(\text{c})} = \left(\alpha_n^{(\text{c})} + \beta_n^{(\text{c})} P_{ij}^{(\sigma)} + \gamma_n^{(\text{c})} P_{ij}^{(\tau)} + \delta_n^{(\text{c})} P_{ij}^{(\sigma)} P_{ij}^{(\tau)} \right) \exp\left[-(r_i - r_j)^2 / a_n^{(\text{c})} \right], \tag{A10}$$

$$V_{ls} = \sum_{n=1}^{2} \sum_{i>j=1}^{A} V_{n,\,ij}^{(ls)}, \tag{A11}$$

TABLE VI. The differences between the used parametrizations of the nuclear potential. Values of $V_{c,3}$ are in MeV.

Parametrization	MHN	NHN	MHN2	NHN2	PHN
$V_{c,3}$	1655	1655	1655	1655	1495
$w_{c,3}$	0.4474	0.5054	0.4474	0.5054	0.575
$m_{c,3}$	0.3985	0.3404	0.3985	0.3404	0.3573
$b_{c,3}$	0.1015	0.1596	0.1015	0.1596	0.1427
$h_{c,3}$	0.0526	-0.0054	0.0526	-0.0054	-0.075
$w_{t,1}$	0.3889	0.3889	0.7015	0.6986	0.7335
$m_{t,1}$	0.6111	0.6111	0.2985	0.3014	0.2665

$$V_{n,\,ij}^{(ls)} = \left(\alpha_n^{(ls)} + \gamma_n^{(ls)} P_{ij}^{(\tau)}\right)[(\mathbf{r}_i - \mathbf{r}_j) \times (\mathbf{p}_i - \mathbf{p}_j)](\mathbf{s}_i + \mathbf{s}_j) \exp\left[-(r_i - r_j)^2 / a_n^{(ls)}\right], \tag{A12}$$

$$V_t = \sum_{n=1}^{3} \sum_{i>j=1}^{A} V_{n,\,ij}^{(t)}, \tag{A13}$$

$$V_{n,\,ij}^{(t)} = 4\left(\alpha_n^{(t)} + \gamma_n^{(t)} P_{ij}^{(\tau)}\right)[3\,(\mathbf{s}_i \mathbf{n}_{ij})\,(\mathbf{s}_j \mathbf{n}_{ij}) - (\mathbf{s}_i \mathbf{s}_j)](r_i - r_j)^2 \exp\left[-(r_i - r_j)^2 / a_n^{(t)}\right]. \tag{A14}$$

Here the following denotations are introduced:

$$\alpha_n^{(c)} = V_{c,n}[w_{c,n} + (1 - g_c)\, m_{c,n}], \quad \beta_n^{(c)} = V_{c,n}\, b_{c,n}, \quad \gamma_n^{(c)} = -V_{c,n}\, h_{c,n}, \quad \delta_n^{(c)} = -g_c\, V_{c,n}\, m_{c,n}, \tag{A15}$$

$$\alpha_n^{(ls)} = g_{ls}\, V_{ls,n}\, w_{ls,n}, \quad \gamma_n^{(ls)} = -g_{ls}\, V_{ls,n}\, m_{ls,n}, \tag{A16}$$

$$\alpha_n^{(t)} = g_t\, V_{t,n}\, w_{t,n}, \quad \gamma_n^{(t)} = -g_t\, V_{t,n}\, m_{t,n}, \tag{A17}$$

$$a_n^{(c)} = \frac{1}{\mu_{c,n}}, \quad a_n^{(ls)} = \frac{1}{\mu_{ls,n}}, \quad a_n^{(t)} = \frac{1}{\mu_{t,n}}, \tag{A18}$$

$$\mathbf{n}_{ij} = \frac{\mathbf{r}_i - \mathbf{r}_j}{|\mathbf{r}_i - \mathbf{r}_j|}, \tag{A19}$$

$P_{ij}^{(\sigma)}$ and $P_{ij}^{(\tau)}$ are the exchange operators, V_n and μ_n are the strength and range parameters, respectively, w_n is the Wigner parameter, and m_n, b_n, and h_n, respectively, are the Majorana, Bartlett, and Heisenberg parameters of the exchange mixtures. Values of these parameters from Ref. [71] are known as the NHN parametrization. Parameter values of the spin-orbit and tensor components from the same Ref. [71] and parameter values of the central one from another Ref. [72] form the MHN parametrization. Actually, the MHN differs from the NHN by the short-range part of the central force. Correcting the long-range part of the tensor force, one obtains the MHN2 and the NHN2 from the MHN and the NHN, respectively. Having also corrected the short-range part of the central force, one can get the PHN. In fact, the MHN2, NHN2, and PHN parametrizations are introduced in the present paper by changing slightly the MHN and the NHN. The corrected parameter values along with the initial ones are collected in Table VI. The others can be found in the original papers [71,72]. The intensity of the central Majorana force (g_c) and the intensities of the spin-orbit (g_{ls}) and tensor (g_t) interactions, which serve as adjustable parameters and vary within reasonable limits, are introduced in the potential (A8) in accordance with work [73].

The generating matrix elements of the central potential (A9) take the form

$$
\begin{aligned}
\langle \mathbf{Q}, s\sigma_f | V_c | \mathbf{R}, s\sigma_i \rangle = \langle \mathbf{Q} | \mathbf{R} \rangle \delta_{\sigma_f \sigma_i} \sum_{n=1}^{3} \left(\varsigma_n^{(c)}\right)^{3/2} \Big\{ & \left(7\alpha_n^{(c)} + \beta_n^{(c)} - \gamma_n^{(c)} - 7\delta_n^{(c)}\right) \\
& + \left[\left(4\alpha_n^{(c)} + 2\beta_n^{(c)} + 2\gamma_n^{(c)} + \delta_n^{(c)}\right) \exp(\mathbf{QR}/2) - 3\alpha_n^{(c)} - \beta_n^{(c)} - 3\gamma_n^{(c)} - 2\delta_n^{(c)}\right] U_n^{(c,+)}(\mathbf{Q}, \mathbf{R}) \\
& - \left[\left(\alpha_n^{(c)} + 2\beta_n^{(c)} + 2\gamma_n^{(c)} + 4\delta_n^{(c)}\right) \exp(\mathbf{QR}/2) - 2\alpha_n^{(c)} - 3\beta_n^{(c)} - \gamma_n^{(c)} - 3\delta_n^{(c)}\right] U_n^{(c,-)}(\mathbf{Q}, \mathbf{R}) \\
& - \left[\left(4\alpha_n^{(c)} + \beta_n^{(c)} - \gamma_n^{(c)} - 4\delta_n^{(c)}\right) \exp(\mathbf{QR}/2) - 2\alpha_n^{(c)} + \beta_n^{(c)} - \gamma_n^{(c)} + 2\delta_n^{(c)}\right] U_n^{(c,0)}(\mathbf{Q}, \mathbf{R}) \Big\},
\end{aligned} \tag{A20}
$$

in which

$$\varsigma_n^{(c)} = \frac{a_n^{(c)}}{2r_0^2 + a_n^{(c)}}, \tag{A21}$$

$$U_n^{(c,\pm,0)}(\mathbf{Q}, \mathbf{R}) = \frac{2}{[\exp(\mathbf{QR}/2) - 1]^2}\, U^{(\pm,0)}\!\left(\varsigma = \sqrt{2r_0^2 \varsigma_n^{(c)} / a_n^{(c)}}, \mathbf{Q}, \mathbf{R}\right). \tag{A22}$$

The generating matrix elements of the spin-orbit potential (A11) can be expressed by

$$\langle \mathbf{Q}, s\sigma_f | V_{ls} | \mathbf{R}, s\sigma_i \rangle = \frac{i}{\sqrt{2}} \langle \mathbf{Q} | \mathbf{R} \rangle \sum_m C^{1\sigma_i}_{1m\ 1\sigma_f} [\mathbf{Q} \times \mathbf{R}]_{1m}$$

$$\times \sum_{n=1}^{2} \left(\varsigma_n^{(ls)}\right)^{5/2} \left\{ \left[(2\alpha_n^{(ls)} + \gamma_n^{(ls)}) \exp(\mathbf{QR}/2) - \alpha_n^{(ls)} - 2\gamma_n^{(ls)} \right] U_n^{(ls,+)}(\mathbf{Q}, \mathbf{R}) \right.$$

$$\left. + \left[(\alpha_n^{(ls)} + 2\gamma_n^{(ls)}) \exp(\mathbf{QR}/2) - 2\alpha_n^{(ls)} - \gamma_n^{(ls)} \right] U_n^{(ls,-)}(\mathbf{Q}, \mathbf{R}) \right\}, \quad (A23)$$

where

$$\varsigma_n^{(ls)} = \frac{a_n^{(ls)}}{2r_0^2 + a_n^{(ls)}}, \quad (A24)$$

$$U_n^{(ls,\pm)} = \frac{2}{[\exp(\mathbf{QR}/2) - 1]^2} U^{(\pm)}\left(\varsigma = \sqrt{2r_0^2 \varsigma_n^{(ls)}/a_n^{(ls)}}, \mathbf{Q}, \mathbf{R}\right). \quad (A25)$$

The generating matrix elements of the tensor potential (A13) can be written as

$$\langle \mathbf{Q}, s\sigma_f | V_t | \mathbf{R}, s\sigma_i \rangle = \sqrt{2\pi}\, \langle \mathbf{Q} | \mathbf{R} \rangle \sum_m C^{1\sigma_f}_{2m\ 1\sigma_i} \sum_{n=1}^{3} \left(\varsigma_n^{(t)}\right)^{7/2} \left(\alpha_n^{(t)} - \gamma_n^{(t)}\right)$$

$$\times \left\{ (\mathbf{Q} + \mathbf{R})^2 Y^*_{2m}(\mathbf{n}_{\mathbf{Q}+\mathbf{R}}) U_n^{(t,+)}(\mathbf{Q}, \mathbf{R}) + (\mathbf{Q} - \mathbf{R})^2 Y^*_{2m}(\mathbf{n}_{\mathbf{Q}-\mathbf{R}}) U_n^{(t,-)}(\mathbf{Q}, \mathbf{R}) \right.$$

$$\left. - (\exp(\mathbf{QR}/2) + 1)\left[Q^2 Y^*_{2m}(\mathbf{n}_{\mathbf{Q}}) U_n^{(t,0)}(Q) + R^2 Y^*_{2m}(\mathbf{n}_{\mathbf{R}}) U_n^{(t,0)}(R) \right] \right\}, \quad (A26)$$

where

$$\varsigma_n^{(t)} = \frac{a_n^{(t)}}{2r_0^2 + a_n^{(t)}}, \quad (A27)$$

$$U_n^{(t,\pm)}(\mathbf{Q}, \mathbf{R}) = \frac{2}{[\exp(\mathbf{QR}/2) - 1]^2} U^{(\pm)}\left(\varsigma = \sqrt{2r_0^2 \varsigma_n^{(t)}/a_n^{(t)}}, \mathbf{Q}, \mathbf{R}\right), \quad (A28)$$

$$U_n^{(t,0)}(Q) = U^{(0)}\left(\varsigma = \sqrt{2r_0^2 \varsigma_n^{(t)}/a_n^{(t)}}, \mathbf{Q}, \mathbf{R} = 0\right), \quad (A29)$$

$$U_n^{(t,0)}(R) = U^{(0)}\left(\varsigma = \sqrt{2r_0^2 \varsigma_n^{(t)}/a_n^{(t)}}, \mathbf{Q} = 0, \mathbf{R}\right). \quad (A30)$$

Substituting the generating matrix elements (A1), (A3), (A4), (A20), (A23), and (A26) into Eq. (15), one can calculate all necessary matrix elements in the basis (6) for the Hamiltonian of the six-nucleon α-d system.

APPENDIX B

The explicit expressions for the generating matrix elements of the E2 and M1 operators at the leading order of the long-wavelength limit for the six-nucleon α-d system in the framework of the developed approach read

$$\langle \mathbf{Q}, s\sigma_f | M^E_{2\mu} | \mathbf{R}, s\sigma_i \rangle = \frac{e\, r_0^2}{12} \delta_{\sigma_f \sigma_i} \left\{ U^{(2)}(\mathbf{Q}, \mathbf{R})(\mathbf{Q} + \mathbf{R})^2 Y_{2\mu}(\mathbf{n}_{\mathbf{Q}+\mathbf{R}}) - \frac{3\, U^{(1)}(\mathbf{Q}, \mathbf{R})}{\exp(\mathbf{QR}/2) - 1} \left[Q^2 Y_{2\mu}(\mathbf{n}_{\mathbf{Q}}) + R^2 Y_{2\mu}(\mathbf{n}_{\mathbf{R}}) \right] \right\}, \quad (B1)$$

$$\langle \mathbf{Q}, s\sigma_f | M^M_{1\mu} | \mathbf{R}, s\sigma_i \rangle = \frac{\mu_N}{12} \sqrt{\frac{3}{\pi}} \left\{ 3\, (g_p + g_n) \sqrt{s(s+1)}\, C^{s\sigma_f}_{s\sigma_i\ 1\mu} U^{(1)}(\mathbf{Q}, \mathbf{R}) - i\, \delta_{\sigma_f \sigma_i} U^{(2)}(\mathbf{Q}, \mathbf{R})[\mathbf{Q} \times \mathbf{R}]_{1\mu} \right\}, \quad (B2)$$

where

$$U^{(1)}(\mathbf{Q}, \mathbf{R}) = \exp(-\mathbf{QR}/3)\,[\exp(\mathbf{QR}/2) - 1]^2, \quad (B3)$$

$$U^{(2)}(\mathbf{Q}, \mathbf{R}) = \exp(-\mathbf{QR}/3)\,[2\exp(\mathbf{QR}/2) + 1]\,[\exp(\mathbf{QR}/2) - 1]. \quad (B4)$$

The generating matrix elements of the components of the E1 operator at the FOLWA are given by

$$\langle \mathbf{Q}, s\sigma_f | \tilde{M}^{E(1)}_{1\mu} | \mathbf{R}, s\sigma_i \rangle = -\frac{e\, k_\gamma^2\, r_0^3}{1080} \delta_{\sigma_f \sigma_i} \left\{ \frac{3\, QR[R\, Y_{1\mu}(\mathbf{n}_{\mathbf{Q}}) + Q\, Y_{1\mu}(\mathbf{n}_{\mathbf{R}})]}{2[\exp(\mathbf{QR}/2) - 1]} \right.$$

$$\left. + [Q\, Y_{1\mu}(\mathbf{n}_{\mathbf{Q}}) + R\, Y_{1\mu}(\mathbf{n}_{\mathbf{R}})]\left(Q^2 + R^2 + 3\, t\, \frac{\partial}{\partial t}\right) \right\} U^{(1)}(\mathbf{Q}, \mathbf{R}), \quad (B5)$$

$$\langle \mathbf{Q}, s\sigma_f | \tilde{M}_{1\mu}^{\text{E(2)}} | \mathbf{R}, s\sigma_i \rangle = -i \frac{\mu_{\text{N}} k_\gamma r_0}{54\sqrt{2}} \delta_{\sigma_f \sigma_i} U^{(2)}(\mathbf{Q}, \mathbf{R}) \sum_{\lambda=0,\pm 1} (-1)^\lambda C_{1\mu \ 1\lambda}^{1(\mu+\lambda)} [\mathbf{Q} \times \mathbf{R}]_{1(-\lambda)} [Q Y_{1(\mu+\lambda)}(\mathbf{n_Q}) + R Y_{1(\mu+\lambda)}(\mathbf{n_R})],$$

$$\tag{B6}$$

$$\langle \mathbf{Q}, s\sigma_f | \tilde{M}_{1\mu}^{\text{E(3)}} | \mathbf{R}, s\sigma_i \rangle = \frac{\mu_{\text{N}} k_\gamma r_0}{6\sqrt{2}} (g_{\text{n}} + g_{\text{p}}) \sqrt{s(s+1)} \, U^{(1)}(\mathbf{Q}, \mathbf{R})$$
$$\times \sum_{\lambda=0,\pm 1} (-1)^\lambda C_{1\mu \ 1\lambda}^{1(\mu+\lambda)} C_{s\sigma_i \ 1(-\lambda)}^{s\sigma_f} [Q Y_{1(\mu+\lambda)}(\mathbf{n_Q}) + R Y_{1(\mu+\lambda)}(\mathbf{n_R})].$$

$$\tag{B7}$$

The generating matrix elements of the E1 operator based on the PEM are expressed by

$$\langle \mathbf{Q}, s\sigma_f | M_{1\mu}^{\text{E(PEM)}} | \mathbf{R}, s\sigma_i \rangle = -e \, r_0 \, \frac{m \, (2m_d - m_\alpha)}{m_d (m_d + m_\alpha)} \delta_{\sigma_f \sigma_i} U^{(1)}(\mathbf{Q}, \mathbf{R}) [Q Y_{1\mu}(\mathbf{n_Q}) + R Y_{1\mu}(\mathbf{n_R})], \tag{B8}$$

where m_d and m_α are the measured masses of the d and α clusters. Obviously, if one sets $m_d = 2m$ and $m_\alpha = 4m$ in accordance with the isospin formalism, one obtains the zero value for Eq. (B8).

The reduced matrix elements of the considered E1, E2, and M1 operators have the form

$$\langle J_f^{\pi_f} l_f s v_f \| M_1^{\text{E(PEM)}} \| J_i^{\pi_i} l_i s v_i \rangle = -e r_0 \frac{m(2m_d - m_\alpha)}{2m_d(m_d + m_\alpha)} \sqrt{\frac{3}{\pi}} \, \Theta_{J_f l_f J_i l_i s}^{(1)} \left(\frac{\kappa_{v_f l_f s}}{\kappa_{v_i l_i s}} \delta_{v_f, v_i-1} + \frac{\kappa_{v_i l_i s}}{\kappa_{v_f l_f s}} \delta_{v_f, v_i+1} \right), \tag{B9}$$

$$\langle J_f^{\pi_f} l_f s v_f \| \tilde{M}_1^{\text{E(1)}} \| J_i^{\pi_i} l_i s v_i \rangle = -\frac{e k_\gamma^2 r_0^3}{1440\sqrt{3\pi}} \, \Theta_{J_f l_f J_i l_i s}^{(1)} \left[2 \frac{\kappa_{v_i l_i s}}{\kappa_{v_f l_f s}} \delta_{v_f, v_i+3} + \left(6 v_i \frac{\kappa_{v_i l_i s}}{\kappa_{v_f l_f s}} + \frac{\tilde{\kappa}_{(v_f-2)l_f s}^2}{\kappa_{v_f l_f s} \kappa_{v_i l_i s}} \right) \delta_{v_f, v_i+1} \right.$$
$$\left. + \left(6 v_f \frac{\kappa_{v_f l_f s}}{\kappa_{v_i l_i s}} + \frac{\tilde{\kappa}_{(v_i-2)l_i s}^2}{\kappa_{v_f l_f s} \kappa_{v_i l_i s}} \right) \delta_{v_f, v_i-1} + 2 \frac{\kappa_{v_f l_f s}}{\kappa_{v_i l_i s}} \delta_{v_f, v_i-3} \right], \tag{B10}$$

$$\langle J_f^{\pi_f} l_f s v_f \| \tilde{M}_1^{\text{E(2)}} \| J_i^{\pi_i} l_i s v_i \rangle = -\frac{\mu_{\text{N}} k_\gamma r_0}{12\sqrt{3\pi}} \, \frac{\bar{\Theta}_{J_f l_f J_i l_i s}}{\kappa_{v_f l_f s} \kappa_{v_i l_i s}} \left[\delta_{v_f, v_i+1} \sum_l \bar{\Omega}_{l_f \, l_i \, l} \tilde{\kappa}_{(v_f-2)ls}^2 + \delta_{v_f, v_i-1} \sum_l \bar{\Omega}_{l_i \, l_f \, l} \tilde{\kappa}_{(v_i-2)ls}^2 \right], \tag{B11}$$

$$\langle J_f^{\pi_f} l_f s v_f \| \tilde{M}_1^{\text{E(3)}} \| J_i^{\pi_i} l_i s v_i \rangle = \frac{\mu_{\text{N}} k_\gamma r_0}{16\sqrt{3\pi}} (g_{\text{n}} + g_{\text{p}}) \bar{\Pi} \, \Theta_{J_f l_f J_i l_i s}^{(1)} \left(\frac{\kappa_{v_i l_i s}}{\kappa_{v_f l_f s}} \delta_{v_f, v_i+1} + \frac{\kappa_{v_f l_f s}}{\kappa_{v_i l_i s}} \delta_{v_f, v_i-1} \right), \tag{B12}$$

$$\langle J_f^{\pi_f} l_f s v_f \| M_2^{\text{E}} \| J_i^{\pi_i} l_i s v_i \rangle = \frac{e r_0^2}{12} \sqrt{\frac{5}{\pi}} \left[\Theta_{J_f l_f J_i l_i s}^{(2)} \left(\frac{\kappa_{v_f l_f s}}{\kappa_{v_i l_i s}} \delta_{v_f, v_i-2} + \frac{\kappa_{v_i l_i s}}{\kappa_{v_f l_f s}} \delta_{v_f, v_i+2} \right) - \sqrt{\frac{15}{2}} \frac{\delta_{v_f v_i}}{\kappa_{v_f l_f s} \kappa_{v_i l_i s}} \sum_l \Omega_{J_f l_f J_i l_i s}^{(2,l)} \tilde{\kappa}_{(v_f-1)ls}^2 \right], \tag{B13}$$

$$\langle J_f^{\pi_f} l_f s v_f \| M_1^{\text{M}} \| J_i^{\pi_i} l_i s v_i \rangle = \frac{\mu_{\text{N}}}{4} \sqrt{\frac{3}{\pi}} \left[(g_{\text{p}} + g_{\text{n}}) \Xi_{J_f l_f J_i l_i s}^{(1)} - \sqrt{\frac{2}{3}} \frac{1}{\kappa_{v_f l_f s} \kappa_{v_i l_i s}} \sum_l \Omega_{J_f l_f J_i l_i s}^{(1,l)} \tilde{\kappa}_{(v_f-1)ls}^2 \right] \delta_{v_f v_i}. \tag{B14}$$

Expressions (B9)–(B14) incorporate the following notations:

$$\Theta_{J_f l_f J_i l_i s}^{(\lambda)} = (-1)^{J_i+l_f+s+\lambda} \Pi_{J_f J_i l_i} C_{l_i 0 \ \lambda 0}^{l_f 0} \begin{Bmatrix} l_i & s & J_i \\ J_f & \lambda & l_f \end{Bmatrix}, \tag{B15}$$

$$\Omega_{J_f l_f J_i l_i s}^{(\lambda, l)} = (-1)^{J_i+l_f+s+\lambda} \Pi_{J_f l_f J_i l_i} C_{l_f 0 \ 10}^{l0} C_{l_i 0 \ 10}^{l0} \begin{Bmatrix} 1 & \lambda & 1 \\ l_f & l & l_i \end{Bmatrix} \begin{Bmatrix} l_i & s & J_i \\ J_f & \lambda & l_f \end{Bmatrix}, \tag{B16}$$

$$\Xi_{J_f l_f J_i l_i s}^{(\lambda)} = (-1)^{J_f+l_f+s+\lambda} \Pi_{J_f J_i s} \sqrt{s(s+1)} \, \delta_{l_f l_i} \begin{Bmatrix} s & l_f & J_i \\ J_f & \lambda & s \end{Bmatrix}, \tag{B17}$$

$$\bar{\Theta}_{J_f l_f J_i l_i s} = (-1)^{J_i+l_f+s+1} \Pi_{J_f l_f J_i l_i} \begin{Bmatrix} l_i & s & J_i \\ J_f & 1 & l_f \end{Bmatrix}, \tag{B18}$$

$$\bar{\Omega}_{l_2 l_1 l} = \sqrt{2l+1} \, C_{l_1 0 \ 10}^{l0} \sum_{l_3} C_{l0 \ 10}^{l_3 0} C_{l_2 0 \ 10}^{l_3 0} \begin{Bmatrix} 1 & 1 & 1 \\ l & l_3 & l_1 \end{Bmatrix} \begin{Bmatrix} 1 & 1 & 1 \\ l_1 & l_3 & l_2 \end{Bmatrix}, \tag{B19}$$

$$\Pi_{j_1 j_2 \dots j_n} = \sqrt{(2j_1+1)(2j_2+1)\dots(2j_n+1)}, \tag{B20}$$

$$\bar{\Pi} = (J_f - J_i)(J_f + J_i + 1) - (l_f - l_i)(l_f + l_i + 1), \tag{B21}$$

$$\kappa_{vls}^2 = \frac{2\pi}{v!}\left[\left(\frac{2}{3}\right)^v - 2\left(\frac{1}{6}\right)^v + \left(-\frac{1}{3}\right)^v\right]\varepsilon_{vl}, \tag{B22}$$

$$\tilde{\kappa}_{vls}^2 = \frac{2\pi}{v!}\left[2\left(\frac{2}{3}\right)^v - \left(\frac{1}{6}\right)^v - \left(-\frac{1}{3}\right)^v\right]\varepsilon_{vl}, \tag{B23}$$

$$\varepsilon_{vl} = \begin{cases} \dfrac{2^{l+1}v![(v+l)/2]!}{(v+l+1)![(v-l)/2]!}, & l \leqslant v, \ \ l+v \ - \ \text{even}, \\ \qquad\qquad 0, & \text{in other cases}, \end{cases} \tag{B24}$$

and $\begin{Bmatrix} a & b & c \\ d & e & f \end{Bmatrix}$ is the $6j$ symbol. The reduced matrix elements (B9)–(B14) are related to the ordinary ones by the Wigner-Eckart theorem [100].

[1] R. H. Cyburt, B. D. Fields, and K. A. Olive, J. Cosmol. Astropart. Phys. 11 (2008) 012.

[2] A. Coc, J.-P. Uzan, and E. Vangioni, J. Cosmol. Astrophys. Phys. 10 (2014) 050.

[3] A. Coc, P. Petitjean, J.-P. Uzan, E. Vangioni, P. Descouvemont, C. Iliadis, and R. Longland, Phys. Rev. D **92**, 123526 (2015).

[4] A. Coc and E. Vangioni, Int. J. Mod. Phys. E **26**, 1741002 (2017).

[5] R. H. Cyburt, B. D. Fields, K. A. Olive, and T.-H. Yeh, Rev. Mod. Phys **88**, 015004 (2016).

[6] S. G. Ryan, T. C. Beers, K. A. Olive, B. D. Fields, and J. E. Norris, Astrophys. J. **530**, L57 (2000).

[7] L. Sbordone, P. Bonifacio, E. Caffau, H.-G. Ludwig, N. T. Behara, J. I. González Hernández et al., Astron. Astrophys. **522**, A26 (2010).

[8] P. D. Serpico, S. Esposito, F. Iocco, G. Mangano, G. Miele, and O. Pisanti, J. Cosmol. Astropart. Phys. 12 (2004) 010.

[9] M. Asplund, D. L. Lambert, P. E. Nissen, F. Primas, and V. V. Smith, Astrophys. J. **644**, 229 (2006).

[10] R. Cayrel, M. Steffen, H. Chand, P. Bonifacio, M. Spite, F. Spite, P. Petitjean, H. G. Ludwig, and E. Caffau, Astron. Astrophys. **473**, L37 (2007).

[11] A. E. García Pérez, W. Aoki, S. Inoue, S. G. Ryan, T. K. Suzuki, and M. Chiba, Astron. Astrophys. **504**, 213 (2009).

[12] K. Lind, J. Melendez, M. Asplund, R. Collet, and Z. Magic, Astron. Astrophys. **554**, A96 (2013).

[13] A. S. Solovyev and S. Yu. Igashov, Phys. Rev. C **96**, 064605 (2017).

[14] A. S. Solovyev and S. Yu. Igashov, Phys. Rev. C **99**, 054618 (2019).

[15] R. G. H. Robertson, P. Dyer, R. A. Warner, R. C. Melin, T. J. Bowles, A. B. McDonald, G. C. Ball, W. G. Davies, and E. D. Earle, Phys. Rev. Lett. **47**, 1867 (1981).

[16] J. Kiener, H. J. Gils, H. Rebel, S. Zagromski, G. Gsottschneider, N. Heide, H. Jelitto, J. Wentz, and G. Baur, Phys. Rev. C **44**, 2195 (1991).

[17] P. Mohr, V. Kölle, S. Wilmes, U. Atzrott, G. Staudt, J. W. Hammer, H. Krauss, and H. Oberhummer, Phys. Rev. C **50**, 1543 (1994).

[18] F. E. Cecil, J. Yan, and C. S. Galovich, Phys. Rev. C **53**, 1967 (1996).

[19] S. B. Igamov and R. Yarmukhamedov, Nucl. Phys. **A673**, 509 (2000).

[20] F. Hammache, M. Heil, S. Typel, D. Galaviz, K. Sümmerer, A. Coc, F. Uhlig, F. Attallah, M. Caamano, D. Cortina, H. Geissel, M. Hellström, N. Iwasa, J. Kiener, P. Koczon, B. Kohlmeyer, P. Mohr, E. Schwab, K. Schwarz, F. Schümann et al., Phys. Rev. C **82**, 065803 (2010).

[21] M. Anders, D. Trezzi, R. Menegazzo, M. Aliotta, A. Bellini, D. Bemmerer, C. Broggini, A. Caciolli, P. Corvisiero, H. Costantini, T. Davinson, Z. Elekes, M. Erhard, A. Formicola, Zs. Fülöp, G. Gervino, A. Guglielmetti, C. Gustavino, Gy. Gyürky, M. Junker, A. Lemut, M. Marta, C. Mazzocchi, P. Prati, C. Rossi Alvarez, D. A. Scott, E. Somorjai, O. Straniero, and T. Szücs, Phys. Rev. Lett. **113**, 042501 (2014).

[22] D. Trezzi, M. Anders, M. Aliotta, A. Bellini, A. Bemmerer, A. Boeltzig et al., Astropart. Phys. **89**, 57 (2017).

[23] K. Langanke and C. Rolfs, Z. Phys. A: At. Nucl. **325**, 193 (1986).

[24] K. Langanke, Nucl. Phys. **A457**, 351 (1986).

[25] R. Crespo, A. M. Eiró, and F. D. Santos, Phys. Rev. C **39**, 305 (1989).

[26] R. Crespo, A. M. Eiró, and J. A. Tostevin, Phys. Rev. C **42**, 1646 (1990).

[27] S. Jang, Phys. Rev. C **47**, 286 (1993).

[28] N. A. Burkova, K. A. Zhaksibekova, M. A. Zhusupov, and R. A. Eramzhyan, Phys. Lett. B **248**, 15 (1990).

[29] S. Typel, G. Blüge, and K. Langanke, Z. Phys. A: Hadrons Nucl. **339**, 335 (1991).

[30] G. G. Ryzhikh, R. A. Eramzhyan, and S. Shlomo, Phys. Rev. C **51**, 3240 (1995); **53**, 2560 (1996).

[31] A. M. Mukhamedzhanov, R. P. Schmitt, R. E. Tribble, and A. Sattarov, Phys. Rev. C **52**, 3483 (1995).

[32] A. M. Mukhamedzhanov, L. D. Blokhintsev, and B. F. Irgaziev, Phys. Rev. C **83**, 055805 (2011).

[33] A. M. Mukhamedzhanov, Shubhchintak, and C. A. Bertulani, Phys. Rev. C **93**, 045805 (2016).

[34] L. D. Blokhintsev, S. B. Igamov, M. M. Nishonov, and R. Yarmukhamedov, Phys. At. Nucl. **69**, 433 (2006) [Yad. Fiz. **69**, 456 (2006)].

[35] A. Kharbach and P. Descouvemont, Phys. Rev. C **58**, 1066 (1998).

[36] K. M. Nollett, R. B. Wiringa, and R. Schiavilla, Phys. Rev. C **63**, 024003 (2001).

[37] L. E. Marcucci, K. M. Nollett, R. Schiavilla, and R. B. Wiringa, Nucl. Phys. **A777**, 111 (2006).

[38] S. B. Dubovichenko and A. V. Dzhazairov-Kakhramanov, Phys. Part. Nucl. **28**, 615 (1997) [Fiz. Elem. Chastits At. Yadra **28**, 1529 (1997)].

[39] S. B. Dubovichenko, Phys. At. Nucl. **73**, 1526 (2010) [Yad. Fiz. **73**, 1573 (2010)].

[40] S. B. Dubovichenko and Yu. N. Uzikov, Phys. Part. Nucl. **42**, 251 (2011) [Fiz. Elem. Chastits At. Yadra **42**, 478 (2011)].

[41] E. M. Tursunov, S. A. Turakulov, and P. Descouvemont, Phys. At. Nucl. **78**, 193 (2015) [Yad. Fiz. **78**, 218 (2015)].

[42] A. Grassi, G. Mangano, L. E. Marcucci, and O. Pisanti, Phys. Rev. C **96**, 045807 (2017).

[43] S. Dubovichenko, A. Dzhazairov-Kakhramanov, and N. Burkova, Int. J. Mod. Phys. E **28**, 1930004 (2019).

[44] E. M. Tursunov, A. S. Kadyrov, S. A. Turakulov, and I. Bray, Phys. Rev. C **94**, 015801 (2016).

[45] E. M. Tursunov, S. A. Turakulov, A. S. Kadyrov, and I. Bray, Phys. Rev. C **98**, 055803 (2018).

[46] D. Baye and E. M. Tursunov, J. Phys. G: Nucl. Part. Phys. **45**, 085102 (2018).

[47] E. M. Tursunov, S. A. Turakulov, and A. S. Kadyrov, Nucl. Phys. **A1000**, 121884 (2020).

[48] P. Navrátil and S. Quaglioni, Phys. Rev. C **83**, 044609 (2011).

[49] G. Hupin, S. Quaglioni, and P. Navrátil, Phys. Rev. Lett. **114**, 212502 (2015).

[50] I. J. Shin, Y. Kim, P. Maris, J. P. Vary, C. Forssén, J. Rotureau, and N. Michel, J. Phys. G: Nucl. Part. Phys. **44**, 075103 (2017).

[51] G. A. Negoita, J. P. Vary, G. R. Luecke, P. Maris, A. M. Shirokov, I. J. Shin, Y. Kim, E. G. Ng, C. Yang, M. Lockner, and G. M. Prabhu, Phys. Rev. C **99**, 054308 (2019).

[52] P. R. Fraser, K. Massen-Hane, A. S. Kadyrov, K. Amos, I. Bray, and L. Canton, Phys. Rev. C **96**, 014619 (2017).

[53] L. D. Blokhintsev and D. A. Savin, Phys. At. Nucl. **77**, 351 (2014) [Yad. Fiz. **77**, 376 (2014)].

[54] L. D. Blokhintsev and D. A. Savin, Phys. At. Nucl. **79**, 358 (2016).

[55] L. D. Blokhintsev, A. S. Kadyrov, A. M. Mukhamedzhanov, and D. A. Savin, Phys. Rev. C **95**, 044618 (2017).

[56] L. D. Blokhintsev, A. S. Kadyrov, A. M. Mukhamedzhanov, and D. A. Savin, Phys. Rev. C **97**, 024602 (2018).

[57] B. K. Luna and T. Papenbrock, Phys. Rev. C **100**, 054307 (2019).

[58] A. S. Solovyev, S. Yu. Igashov, and Yu. M. Tchuvil'sky, Phys. At. Nucl. **77**, 1453 (2014) [Yad. Fiz. **77**, 1525 (2014)].

[59] A. S. Solovyev, S. Yu. Igashov, and Y. Yu. Tchuvil'sky, J. Phys.: Conf. Ser. **569**, 012020 (2014).

[60] A. S. Solovyev, S. Yu. Igashov, and Yu. M. Tchuvil'sky, EPJ Web Conf. **86**, 00054 (2015).

[61] A. S. Solovyev, S. Yu. Igashov, and Yu. M. Tchuvil'sky, EPJ Web Conf. **117**, 09017 (2016).

[62] A. M. Shirokov, A. I. Mazur, I. A. Mazur, and J. P. Vary, Phys. Rev. C **94**, 064320 (2016).

[63] A. M. Shirokov, G. Papadimitriou, A. I. Mazur, I. A. Mazur, R. Roth, and J. P. Vary, Phys. Rev. Lett. **117**, 182502 (2016).

[64] K. Kravvaris and A. Volya, Phys. Rev. Lett. **119**, 062501 (2017).

[65] K. Kravvaris and A. Volya, Phys. Rev. C **100**, 034321 (2019).

[66] V. S. Vasilevsky, K. Katō, and N. Zh. Takibayev, Phys. Rev. C **96**, 034322 (2017).

[67] V. S. Vasilevsky, Yu. A. Lashko, and G. F. Filippov, Phys. Rev. C **97**, 064605 (2018).

[68] V. S. Vasilevsky, K. Katō, and N. Takibayev, Phys. Rev. C **98**, 024325 (2018).

[69] A. D. Duisenbay, N. Kalzhigitov, K. Katō, V. O. Kurmangaliyeva, N. Takibayev, and V. S. Vasilevsky, Nucl. Phys. **A996**, 121692 (2020).

[70] M. Freer, H. Horiuchi, Y. Kanada-En'yo, D. Lee, and U.-G. Meißner, Rev. Mod. Phys. **90**, 035004 (2018).

[71] H. Kanada, T. Kaneko, S. Nagata, and M. Nomoto, Prog. Theor. Phys. **61**, 1327 (1979).

[72] F. Tanabe, A. Tohsaki, and R. Tamagaki, Prog. Theor. Phys. **53**, 677 (1975).

[73] T. Kajino, T. Matsuse, and A. Arima, Nucl. Phys. A **413**, 323 (1984).

[74] D. Baye, Phys. Rev. C **86**, 034306 (2012).

[75] P. Raghavan, At. Data Nucl. Data Tables **42**, 189 (1989).

[76] J. Cederberg, D. Olson, J. Larson, G. Rakness, K. Jarausch, J. Schmidt, B. Borovsky, P. Larson, and B. Nelson, Phys. Rev. A **57**, 2539 (1998).

[77] D. R. Tilley, C. M. Cheves, J. L. Godwin, G. M. Hale, H. M. Hofmann, J. H. Kelley, C. G. Sheu, and H. R. Weller, Nucl. Phys. **A708**, 3 (2002).

[78] G. Audi, A. H. Wapstra, and C. Thibault, Nucl. Phys. **A729**, 337 (2003).

[79] I. Tanihata, H. Savajols, and R. Kanungo, Prog. Part. Nucl. Phys. **68**, 215 (2013).

[80] M. P. Bornand, G. R. Plattner, R. D. Viollier, and K. Alder, Nucl. Phys. **A294**, 492 (1978).

[81] F. D. Santos, I. J. Thompson, and A. M. Eiró, J. Phys. Colloq. **51**, C6-443 (1990).

[82] L. D. Blokhintsev, V. I. Kukulin, A. A. Sakharuk, D. A. Savin, and E. V. Kuznetsova, Phys. Rev. C **48**, 2390 (1993).

[83] K. D. Veal, C. R. Brune, W. H. Geist, H. J. Karwowski, E. J. Ludwig, A. J. Mendez E. E. Bartosz, P. D. Cathers, T. L. Drummer, K. W. Kemper, A. M. Eiró, F. D. Santos, B. Kozlowska, H. J. Maier, and I. J. Thompson, Phys. Rev. Lett. **81**, 1187 (1998).

[84] E. A. George and L. D. Knutson, Phys. Rev. C **59**, 598 (1999).

[85] H. R. Weller and D. R. Lehman, Ann. Rev. Nucl. Part. Sci. **38**, 563 (1988).

[86] A. M. Eiró and F. D. Santos, J. Phys. G: Nucl. Part. Phys. **16**, 1139 (1990).

[87] V. Punjabi, C. F. Perdrisat, E. Cheung, J. Yonnet, M. Boivin, E. Tomasi-Gustafsson, R. Siebert, R. Frascaria, E. Warde, S. Belostotsky, O. Miklucho, V. Sulimov, R. Abegg, and D. R. Lehman, Phys. Rev. C **46**, 984 (1992).

[88] P. R. Dee, C. O. Blyth, H. D. Choi, N. M. Clarke, S. J. Hall, O. Karban, I. Martel-Bravo, S. Roman, G. Tungate, R. P. Ward, N. J. Davis, D. B. Steski, K. A. Connell, and K. Rusek, Phys. Rev. C **51**, 1356 (1995).

[89] K. Rusek, N. M. Clarke, G. Tungate, and R. P. Ward, Phys. Rev. C **52**, 2614 (1995).

[90] P. V. Green, K. W. Kemper, P. L. Kerr, K. Mohajeri, E. G. Myers, D. Robson, K. Rusek, and I. J. Thompson, Phys. Rev. C **53**, 2862 (1996).

[91] L. C. McIntyre and W. Haeberli, Nucl. Phys. **A91**, 382 (1967).

[92] L. G. Keller and W. Haeberli, Nucl. Phys. A **156**, 465 (1970).

[93] P. A. Schmelzbach, W. Grüebler, V. König, and P. Marmier, Nucl. Phys. A **184**, 193 (1972).

[94] W. Grüebler, P. A. Schmelzbach, V. König, R. Risler, and D. Boerma, Nucl. Phys. **A242**, 265 (1975).

[95] B. Jenny, W. Grüebler, V. König, P. A. Schmelzbach, and C. Schweizer, Nucl. Phys. **A397**, 61 (1983).

[96] D. R. Thompson and Y. C. Tang, Phys. Rev. C **8**, 1649 (1973).

[97] H. Kanada, T. Kaneko, and Y. C. Tang, Nucl. Phys. **A389**, 285 (1982).

[98] H. Kanada, T. Kaneko, S. Saito, and Y. C. Tang, Nucl. Phys. **A444**, 209 (1985).

[99] Y. Fujiwara and Y. C. Tang, Phys. Rev. C **43**, 96 (1991).

[100] D. A. Varshalovich, A. N. Moskalev, and V. K. Khersonskii, *Quantum Theory of Angular Momentum* (World Scientific Publishing, Singapore, 1988).